A Kv2 inhibitor combination reveals native neuronal conductances consistent with Kv2/KvS heteromers.

Robert G. Stewart[1,2,3], Matthew James Marquis[1], Sooyeon Jo[3], Aman Aberra[2,4], Verity Cook[2,5], Zachary Whiddon[2], Michael Ferns[1,6], Jon T. Sack[1,2,6]

Affiliations:
[1] Department of Physiology and Membrane Biology, University of California Davis
[2] Neurobiology Course, Marine Biological Laboratory, Woods Hole, Massachusetts
[3] Department of Neurobiology, Harvard Medical School, Boston, Massachusetts
[4] Department of Biological Sciences, Dartmouth College, Hanover, New Hampshire
[5] Einstein Center for Neuroscience, Charité Universitätsmedizin Berlin, Germany
[6] Department of Anesthesiology and Pain Medicine, University of California Davis

Corresponding author email: jsack@ucdavis.edu

Conflict of interest statement: The authors declare no conflicts of interest.

ABSTRACT

KvS proteins are voltage-gated potassium channel subunits that form functional channels when assembled into heterotetramers with Kv2.1 (*KCNB1*) or Kv2.2 (*KCNB2*). Mammals have 10 KvS subunits: Kv5.1 (*KCNF1*), Kv6.1 (*KCNG1*), Kv6.2 (*KCNG2*), Kv6.3 (*KCNG3*), Kv6.4 (*KCNG4*), Kv8.1 (*KCNV1*), Kv8.2 (*KCNV2*), Kv9.1 (*KCNS1*), Kv9.2 (*KCNS2*), and Kv9.3 (*KCNS3*). Electrically excitable cells broadly express channels containing Kv2 subunits and most neurons have substantial Kv2 conductance. However, whether KvS subunits contribute to these conductances has not been clear, leaving the physiological roles of KvS subunits poorly understood. Here, we identify that two potent Kv2 inhibitors, used in combination, can distinguish conductances of Kv2/KvS channels and Kv2-only channels. We find that Kv5, Kv6, Kv8, or Kv9-containing channels are resistant to the Kv2-selective pore-blocker RY785 yet remain sensitive to the Kv2-selective voltage sensor modulator guangxitoxin-1E (GxTX). Using these inhibitors in mouse superior cervical ganglion neurons, we find that little of the Kv2 conductance is carried by KvS-containing channels. In contrast, conductances consistent with KvS-containing channels predominate over Kv2-only channels in mouse and human dorsal root ganglion neurons. These results establish an approach to pharmacologically distinguish conductances of Kv2/KvS heteromers from Kv2-only channels, enabling investigation of the physiological roles of endogenous KvS subunits. These findings suggest that drugs targeting KvS subunits could modulate electrical activity of subsets of Kv2-expressing cell types.

INTRODUCTION

The Kv2 voltage-gated K^+ channel subunits, Kv2.1 and Kv2.2, are broadly expressed in electrically excitable cells throughout the body and have important ion-conducting and non-conducting functions (Trimmer, 1993; Du et al., 2000; Li et al., 2013; Liu and Bean, 2014; Bishop et al., 2015; Johnson et al., 2018; Kirmiz et al., 2018; Vierra et al., 2021; Matsumoto et al., 2023). Consistent with this widespread expression, Kv2 channels have profound impacts on many aspects of our physiology including vision, seizure suppression, stroke recovery, pain signaling, blood pressure, insulin secretion, and reproduction (Bocksteins, 2016). Although modulation of Kv2 channels may seem to hold therapeutic promise, Kv2 subunits are poor drug targets due to their importance in many tissues.

A potential source of molecular diversity for Kv2 channels are a family of Kv2-related proteins referred to as regulatory, silent, or KvS subunits (Bocksteins et al., 2009; Kobertz, 2018). KvS subunits are an understudied class of voltage-gated K^+ channel (Kv) subunits that comprise one fourth of mammalian Kv subunit types. Like all other Kv proteins, the ten KvS proteins (Kv5.1, Kv6.1-6.4, Kv8.1-8.2, and Kv9.1-9.3) have sequences encoding a voltage sensor and pore domain. Distinct from other Kv subunits, KvS have not been found to form functional homomeric channels. Rather, KvS subunits co-assemble with Kv2 subunits to form heterotetrameric Kv2/KvS channels (Salinas et al., 1997a; Kramer et al., 1998) which have biophysical properties distinct from those of homomeric Kv2 channels (Post et al., 1996; Salinas et al., 1997b; Kramer et al., 1998; Richardson and Kaczmarek, 2000; Zhong et al., 2010; Bocksteins et al., 2012; Bocksteins et al., 2017). KvS mRNAs are expressed in tissue and cell-specific manners that overlap with Kv2.1 or Kv2.2 expression (Castellano et al., 1997; Salinas et al., 1997b; Kramer et al., 1998; Bocksteins et al., 2012; Bocksteins and Snyders, 2012; Bocksteins, 2016). These expression patterns and functional effects suggest that Kv2 conductances in many cell types might be Kv2/KvS conductances. Consistent with narrow expression of the many KvS subunits, genetic mutations and gene-targeting studies have linked disruptions in the function of different KvS subunits to defects in distinct organ systems including retinal cone dystrophy (Wu et al., 2006; Hart et al., 2019; Inamdar et al., 2022), male infertility (Regnier et al., 2017), seizures (Jorge et al., 2011), and changes in pain sensitivity (Tsantoulas et al., 2018) (Lee et al., 2020b). These organ-specific disruptions suggest that each KvS subunit selectively modulates a subset of the wide-ranging functions of Kv2 channels. However, studies of the physiological roles of KvS subunits have been hindered by a lack of tools to identify native KvS conductances. Due to limited KvS pharmacology, there is little evidence that definitively ascribes native K^+ conductances to KvS-containing channels. While studies have identified native conductances attributed to KvS subunits (reviewed by Bocksteins, 2016), it has not been clear whether the Kv2 conductances that are prominent in many electrically-excitable cell types are carried by Kv2-only channels, or Kv2/KvS heteromeric channels.

No drugs are known to be selective for KvS subunits. However, Kv2/KvS heteromeric channels do have some pharmacology distinct from channels that contain only Kv2 subunits. Quaternary ammonium compounds, 4-aminopyridine, and other broad-spectrum K^+ channel blockers have different potencies against certain KvS-containing channels as compared to Kv2 channels (Post et al., 1996; Thorneloe and Nelson, 2003; Stas et al., 2015). However, these blockers are poorly selective and cannot effectively isolate Kv2/KvS conductances from the many other voltage-gated K^+ conductances of electrically excitable cells.

Highly-selective Kv2 channel inhibitors fall into two mechanistically distinct classes. One class is the inhibitory cystine knot peptides from spiders. An exemplar of this class is the tarantula toxin guangxitoxin-1E (GxTX), which has remarkable specificity for Kv2 channel subunits over other voltage-gated channels (Herrington et al., 2006; Thapa et al., 2021). GxTX binds to the voltage sensor of each Kv2 subunit (Milescu et al., 2009), and stabilizes that voltage sensor in a resting state to prevent channel opening (Tilley et al., 2019). GxTX binding requires a specific sequence of residues, TIFLTES, at the extracellular end of the Kv2 subunit S3 transmembrane helix (Milescu et al., 2013). This GxTX-binding sequence is conserved between

Kv2 channels but is not retained by any KvS subunit. A second class of selective Kv2 inhibitors is a family of small molecules discovered in a high throughput screen for use-dependent Kv2 inhibitors (Herrington et al., 2011). Of these, RY785 is the most selective for Kv2 channels over other channel types. RY785 acts like a pore blocker which binds in the central cavity of Kv2 channels (Marquis and Sack, 2022). The central cavity-lining residues of all KvS subunits have differences from Kv2 subunits. We recently reported that coexpression of Kv5.1 with Kv2.1 led to a conductance that was resistant to RY785 (Ferns et al., 2024).

In this study, we develop a method to isolate conductances of KvS-containing channels. We identify that the combination of GxTX and RY785 can distinguish conductances of Kv2-only channels from channels that contain KvS subunits of the Kv5, Kv6, Kv8, or Kv9 subfamilies. To determine whether cell types enriched with KvS mRNA have functional KvS-containing channels, we use these inhibitors to reveal native neuronal conductances consistent with Kv2/KvS heteromers in mouse and human dorsal root ganglion neurons. These findings suggest that KvS conductances could be targeted to selectively modulate discrete subsets of cell types.

RESULTS

- Kv2.1/Kv8.1 heteromers are resistant to RY785 and sensitive to GxTX

To test whether Kv2 inhibitors also inhibit Kv2/KvS heteromeric channels, we transfected KvS cDNA into a stable cell line which was subsequently induced to express Kv2.1 (Kv2.1-CHO) (Figure 1 Supplement) and later recorded whole cell currents. We previously found that 1 µM RY785 or 100 nM GxTX blocked almost all the voltage-gated K^+ conductance of this Kv2.1-CHO cell line, leaving 1 ± 2% or 0 ± 0.1% (mean ± SEM) current remaining respectively at 0 mV (Tilley et al., 2019; Marquis and Sack, 2022). However, after transfection of Kv8.1 into Kv2.1-CHO cells, we find that a sizable component of the delayed rectifier current became resistant to 1 µM RY785 (Fig 1 A). This RY785-resistant current was inhibited by 100 nM GxTX, suggesting that the GxTX-sensitivity arises from inclusion of Kv2.1 subunits in the channels underlying the RY785-resistant current. A simple interpretation is that RY785-resistant yet GxTX-sensitive currents are carried by Kv2.1/Kv8.1 heteromeric channels. The fraction of RY785-resistant current had pronounced cell-to-cell variability (Fig 1 D). Co-expression of KvS and Kv2 subunits can result in Kv2 homomers and Kv2/KvS heteromers (Pisupati et al., 2018), so variability in the RY785-sensitive fraction could represent cell-to-cell variability in the proportion of Kv8.1-containing channels.

As a control, we transfected Kv2.1-CHO cells with Navβ2, a transmembrane protein not expected to interact with Kv2.1. In Kv2.1-CHO cells transfected with Navβ2, 1 µM RY785 efficiently blocked Kv2.1 conductance, leaving 4 ± 0.6 % (mean ± SEM) of current (Fig 1 B and D). We also transfected Kv2.1-CHO cells with a member of the AMIGO family of Kv2-regulating transmembrane proteins. AMIGO1 promotes voltage sensor activation of Kv2.1 channels in these Kv2.1-CHO cells (Sepela et al., 2022). 1 µM RY785 blocked Kv2.1 conductances in cells transfected with AMIGO1, leaving 0.6 ± 1% (SEM) of current (Fig 1 C and D). These control experiments indicate that transfection of a set of other transmembrane proteins did not confer resistance to RY785, suggesting that the RY785 resistance is not generically induced by overexpression of non-KvS transmembrane proteins.

To determine whether Kv8.1-containing channels are completely resistant to RY785, we performed an RY785 concentration-effect experiment. To pre-block Kv2.1 homomers we began concentration-effect measurements at 0.35 µM RY785, which we expect to block 98% of homomers based on the estimated K_D of 6 nM RY785 for the Kv2.1 currents in these Kv2.1-CHO cells (Marquis and Sack, 2022). Notably, currents resistant to 0.35 µM RY785 were blocked by higher concentrations of RY785, with nearly complete block observed in 35 µM RY785 (Fig 2 A). We quantified block of tail currents at -9 mV following a 200 ms step to +71 mV, and normalized to current from the initial 0.35 µM RY785 treatment. This protocol revealed an IC_{50} of 5 ± 1 µM (SD) (Fig 2 B). The Hill coefficient of 1.2 ± 0.2 is consistent with 1:1 binding to a homogenous population of RY785-inhibited channels.

We had noted that solution exchanges can change current amplitudes, and also interleaved time-matched solution exchange controls. These controls revealed variable current rundown of approximately 30% on average (Fig 2 C). Time-matched control washes were followed by treatment with 35 µM RY785 to confirm that currents in these cells had similar RY785 sensitivity to those in our concentration-effect experiment. Following block by 35 µM RY785, washing with 0.35 µM RY785 caused increases in current amplitudes in every trial (Fig 2 D). The run-down and incomplete wash-out indicate that the 5 µM IC_{50} of RY785 for these resistant channels may be an underestimate. Kv2.1/Kv8.1 currents were unblocked in the first current test following RY785 washout (Fig 2 Supplement). This rapid recovery indicates unblocking of Kv2.1/Kv8.1 heteromers occurred during the less than 3 min wash time at -89 mV, or if RY785 remained trapped in the channels during wash then it unblocked on the millisecond time scale during activating voltage pulses. This is distinct from Kv2.1 homomers, where RY785 becomes trapped in deactivated channels and unblocks much more slowly, with a time constant of about 2 hours

at -92 mV or 100 s at +28 mV (Marquis and Sack, 2022). The dramatically faster unblock from Kv2.1/Kv8.1 is consistent with the weaker affinity observed for RY785. Overall, the results suggest that Kv8.1-containing channels in these Kv2.1-CHO cells form a pharmacologically-homogenous population with an affinity for RY785 ~3 orders of magnitude weaker than for Kv2.1 homomers. Our estimates of the affinities of Kv2.1 homomeric and Kv2.1/Kv8.1 heteromeric channels for RY785 suggest that ~1 µM RY785 elicits nearly complete block of Kv2.1 homomer conductance while blocking little Kv2.1/KvS heteromer conductance.

- Biophysical properties of RY785-resistant conductance are consistent with Kv2.1/Kv8.1 channels.

We wondered whether RY785 block of Kv2 homomers could better reveal the gating of heteromers. While concentrations of RY785 that partially block Kv2.1/Kv8.1 modified the kinetics of voltage-dependent gating, suggesting state-dependent block (Fig 3), we did not observe modification of kinetics with 3.5 µM or lower concentrations of RY785. To study the biophysical properties of the Kv8.1 conductance in the Kv2.1-CHO cells, we analyzed currents in 1 µM RY785 to block the Kv2.1 homomers. For comparison, Kv2.1-CHO cells were transfected with a control plasmid and treated with a vehicle control (Fig 4 Supplement 1). We stepped cells to -9 mV from a holding potential of -89 mV and fit the current rise with an exponential function (equation 1). Cells transfected with Kv8.1 and blocked with 1 µM RY785 had a significantly slower activation time constant and lower sigmoidicity (shorter relative activation delay) than Kv2.1 (Fig 4 A-C). Conductance-voltage relations were fit with a Boltzmann function (equation 2) revealing that the half-maximal conductance of Kv8.1-transfected cells is shifted positive relative to Kv2.1 alone (Fig 4 D and E). We did not detect a significant difference in the steepness (z) of the conductance voltage relation (Fig 4 F). Currents from Kv8.1-transfected cells inactivated less during a 10 s step to -9 mV (Fig 4 G and H). However, the steady-state inactivation of Kv8.1-transfected cells was shifted to more negative voltages and is less steep than Kv2.1-transfected cells (Fig 4 I-K). These biophysical properties are consistent with a previous report which identified that co-expression of Kv8.1 with Kv2.1 in *Xenopus* oocytes slows the rate of activation, reduces inactivation and shifts steady-state inactivation to more negative voltages (Salinas et al., 1997b). This previous report also identified a positive shift in the conductance-voltage relation when Kv8.1 is co-expressed with a Kv2 subunit (Kv2.2), similar to our findings with Kv2.1/Kv8.1. Together these results show that RY785-resistant currents in cells transfected with Kv8.1 are distinct from Kv2.1 and have changes in gating consistent with the prior reports of Kv8.1/Kv2 biophysics. This validates using RY785 block of Kv2 homomers as a method to reveal the biophysics of a Kv8.1-containing population.

- A subunit from each KvS family is resistant to RY785 but sensitive to GxTX.

To test if RY785 resistance is shared broadly by KvS subunits, we studied a subunit from each KvS subfamily. We previously found that the sole Kv5 subunit, Kv5.1, was resistant to RY785 (Ferns et al., 2024). We transfected Kv5.1, Kv6.4, and Kv9.3, to find if they also produced delayed rectifier current resistant to 1 µM RY785 yet sensitive to 100 nM GxTX (Fig 5 A-C). We observed that, in 1 µM RY785, >10% of the voltage-gated current remained in 12/13 Kv5.1, 9/14 Kv6.4, and 5/5 Kv9.3 transfected cells (Fig 5 D). Like Kv8.1, the fraction of RY785-resistant current had pronounced cell-to-cell variability (Fig 5 D) suggesting that the RY785-sensitive fraction could be due to different ratios of functional Kv2.1 homomers to Kv2.1/KvS heteromers. Addition of 100 nM GxTX blocked RY785-resistant current from cells transfected with each of these KvS subunits. A slightly higher fraction of Kv9.3 current remained in 100 nM GxTX, possibly due to Kv9.3 negatively shifting the midpoint of the conductance voltage

relationship (Kerschensteiner and Stocker, 1999). These results show that voltage-gated outward currents in cells transfected with members from each KvS family have decreased sensitivity to RY785 but remain sensitive to GxTX. While we did not test every KvS regulatory subunit, the ubiquitous resistance across all KvS subfamilies results suggest that all KvS subunits may provide resistance to 1 µM RY785 yet remain sensitive to GxTX, and that resistance is a hallmark of KvS-containing channels.

- The Kv2 conductances of mouse superior cervical ganglion neurons do not have KvS-like pharmacology.

We set out to assess whether RY785 together with GxTX could be a means of distinguishing endogenous Kv2/KvS channels from Kv2 channels in native neurons. We first designed experiments to test whether RY785 could inhibit endogenous Kv2 currents in mice, by studying neurons unlikely to express KvS subunits. Rat superior cervical ganglion (SCG) neurons have robust GxTX-sensitive conductances (Liu and Bean, 2014) yet transcriptomics have revealed little evidence of KvS expression (Sapio et al., 2020). We investigated whether SCG neurons have KvS-like conductances by performing whole cell voltage clamp on dissociated mouse neurons. To help isolate Kv2 and Kv2/KvS currents, we bathed SCG neurons in a cocktail of Nav, Kv1, Kv3, and Kv4 inhibitors and recorded voltage-gated currents. We found that exposing SCG neurons to 1 µM RY785 inhibited most of the voltage-gated current, and subsequent addition of 100 nM GxTX inhibited little additional current (Fig 6 A and B). To quantify inhibition, we analyzed tail currents 10 ms after repolarizing to -45 mV, as a hallmark of Kv2 currents is relatively slow deactivation (Thorneloe and Nelson, 2003; Zheng et al., 2019). Tail currents after application of 1 µM RY785 were decreased by 88 $\pm$ 5 % (mean $\pm$ SEM) in SCG neurons (Fig 6 B). Subsequent application of 100 nM GxTX had little further effect. To determine if the RY785-sensitive conductances are consistent with previous reports of Kv2 channels, we examined the biophysical properties of the Kv2-like (RY785-sensitive) currents defined by subtraction (Fig 6 C). Current activation began to be apparent at -45 mV and had a conductance that was half maximal at -11 mV (Fig 6 D). The faster component of deactivation of RY785-sensitive currents in SCG neurons had a time constant of 16 ms $\pm$ 0.6 (mean $\pm$ SEM) at -45 mV (Fig 6 E). These results are consistent with reported biophysical properties of Kv2 channels (Kramer et al., 1998; Liu and Bean, 2014; Tilley et al., 2019; Sepela et al., 2022). Together these results show that 1 µM RY785 almost completely inhibits endogenous Kv2-like conductances in these mouse neurons, suggesting that mouse SCG neurons have few functional Kv2/KvS channels. We cannot rule out that the small amount of current remaining after RY785 (12% of the control) is due to Kv2/KvS channels, but its insensitivity to GxTX suggests that it may instead be current from a non-Kv2 channel remaining in the cocktail of K-channel inhibitors.

- Mouse nociceptors have KvS-like conductances.

To determine if RY785/GxTX pharmacology could reveal endogenous KvS-containing channels, we next studied neurons likely to express KvS subunits. Mouse DRG somatosensory neurons express Kv2 proteins (Stewart et al., 2024), have GxTX-sensitive conductances (Zheng et al., 2019), and express a variety of KvS transcripts (Bocksteins et al., 2009; Zheng et al., 2019). To record from a consistent subpopulation of mouse somatosensory neurons, we used a *Mrgprd*^{GFP} transgenic mouse line which expresses GFP in nonpeptidergic nociceptors (Zylka et al., 2005; Zheng et al., 2019). Deep sequencing identified that mRNA transcripts for Kv5.1, Kv6.2, Kv6.3, and Kv9.1 are present in GFP^{+} neurons of this mouse line (Zheng et al., 2019) and we confirmed the presence of Kv5.1 and Kv9.1 transcripts in GFP^{+} neurons from *Mrgprd*^{GFP} mice using RNAscope (Fig 7 Supplement 1). We investigated whether these neurons have KvS-

like conductances by performing whole cell voltage clamp on cultured DRG neurons that had clear GFP fluorescence. Voltage-clamped neurons were bathed in the same cocktail of channel inhibitors used on SCG neurons with the addition of a Nav1.8 inhibitor, A-803467. Application 1 µM RY785 inhibited outward currents somewhat, but unlike in SCG neurons, a prominent delayed-rectifier outward conductance with slow deactivation remained (Fig 7 A left panel). Tail currents in 1 µM RY785 decreased 29 ± 3% (mean ± SEM) (Fig 7 B left panel). Subsequent application of 100 nM GxTX decreased tail currents by 68 ± 5% (mean ± SEM) of their original amplitude before RY785. We observed variable current run-up or run-down but no significant effect of vehicle in blinded, interleaved experiments, while RY785 significantly decreased tail currents relative to vehicle controls (Fig 7 A and B right panel). Concurrent application of 100 nM GxTX and 1 µM RY785 to neurons in vehicle decreased currents by 69 ± 5% (mean ± SEM).

To determine if the RY785- and GxTX-sensitive conductances in GFP^+ neurons from *Mrgprd*^{GFP} mice are consistent with previous reports of Kv2- or KvS-containing channels, we examined the biophysical properties of the Kv2-like (RY785-sensitive) and KvS-like (RY785-resistant, GxTX-sensitive) currents defined by subtraction (Fig 7 C). Obvious Kv2-like and KvS-like channel conductances began at -44 mV and had half-maximal conductances around -19 mV (Fig 7 D), consistent with Kv2 and many KvS-containing channels (Kramer et al., 1998; Richardson and Kaczmarek, 2000; Sano et al., 2002; Thorneloe and Nelson, 2003). Moreover, KvS-like, GxTX-sensitive currents deactivated slower than Kv2-like, RY785-sensitive currents (Fig 7 E), consistent with the effects of several KvS subunits whose transcripts are expressed in nociceptor DRG neurons. Kv5.1, Kv6.3, and Kv9.1 all slow deactivation of Kv2 conductances in heterologous cells (Salinas et al., 1997a; Kramer et al., 1998; Sano et al., 2002), and in Kv2.1-CHO cells transfected with Kv5.1, we confirmed that RY785-resistant currents deactivate slower than Kv2.1 controls (Fig 7 Supplement 2). Together, these results indicate that, in these mouse DRG neurons, RY785-sensitive currents are Kv2-like, while RY785-resistant yet GxTX-sensitive currents are KvS-like. Of the total conductance sensitive to RY785 + GxTX, 58 ± 3 % (mean ± SEM) was resistant to RY785 (KvS-like) (Fig 7 F). Overall, these results show that these non-peptidergic nociceptor DRG neurons from mice have KvS transcripts and endogenous voltage-gated currents with KvS-like pharmacology and gating.

- Human somatosensory neurons have KvS-like conductances.

Human DRG neurons express Kv2 proteins (Stewart et al., 2024), and express KvS transcripts (Ray et al., 2018) suggesting that they may have Kv2/KvS conductances. We performed whole-cell voltage clamp on cultured human DRG neurons, choosing smaller-diameter neurons and using the same solutions as mouse DRG neuron recordings. The human DRG neurons had KvS-like delayed-rectifier outward conductances that were sensitive to 100 nM GxTX that were insensitive to 1 µM RY785 (Fig 8 A, B, C). These RY785- or GxTX-sensitive conductances became apparent near -44 mV and were half-maximal between -14 and -4 mV (Fig 8 D). Of the total conductance sensitive to RY785 or GxTX in these human DRG neurons, 76 ± 2 % (mean ± SEM) was KvS-like, being resistant to RY785 but sensitive to GxTX (Fig 8 E). Overall, these results show that human DRG neurons can produce endogenous voltage-gated currents with pharmacology and gating consistent with Kv2/KvS channels.

DISCUSSION

These results identify a method for pharmacologically isolating conductances of Kv2/KvS channels and Kv2-only channels. RY785 blocks homomeric Kv2 channels, and subsequent application of GxTX selectively inhibits Kv2/KvS-containing channels. Such a protocol can aid in identification of Kv2/KvS conductances separately from the Kv2 homomer conductances that are likely to be in the same cell. Characterization of these now separable conductances can reveal impacts of Kv2-only channels and KvS-containing channels on electrophysiological signaling. This is valuable as there are few other tools to probe the contributions of KvS subunits to electrical signaling in native cells and tissues.

It is remarkable that resistance to RY785 is shared across all of the KvS families. We found Kv2.1/Kv8.1 conductances to be ~1000 times less sensitive to RY785 than Kv2.1 homomer conductances in the same cell line. Based on the observation that >50% of Kv current was resistant to 1 µM RY785 in some Kv2.1-CHO cells transfected with Kv5.1, Kv6.4, or Kv9.3, these Kv2.1/KvS channels are expected to have IC_{50} > 1 µM, at least 100-fold less sensitive than the ~10 nM IC_{50} for Kv2.1 in this cell line. This could suggest that the RY785 inhibitory site is substantially disrupted by KvS subunits. Site disruption by KvS subunits could result from steric change in the binding site itself or could be allosteric. In Kv2.1 homomeric channels, intracellular tetraethylammonium competes with RY785 inhibition, and voltage gates RY785 access to its inhibitory site, suggesting that RY785 binds within the voltage-gated intracellular cavity lined by transmembrane segment S6 helices. In all KvS subunits, the S6 residues lining this cavity are distinct (Marquis and Sack, 2022). The precise subunit compositions of KvS-containing channels are debated, with evidence for KvS:Kv2 stoichiometries of either 1:3 (Kerschensteiner et al., 2005; Pisupati et al., 2018) or 2:2 (Moller et al., 2020). If KvS subunits sterically disrupt the RY785 site, this would suggest that the RY785 site spans multiple Kv2 subunits, at least one of which is replaced in the Kv2/KvS heteromers. If the KvS disruption of RY785 inhibition is allosteric, KvS subunits would reduce the occurrence of channel state(s) which bind most tightly to RY785. Allosteric interactions between RY785 inhibition and channel gating are apparent for Kv2.1 homomeric channels as RY785 alters voltage-sensor movement, indicating that RY785 affinity must be state-dependent (Marquis and Sack, 2022). We note that the altered Kv2.1/Kv8.1 conductance kinetics in 35 µM RY785 are consistent with state-dependent binding (Fig. 3). An allosteric mechanism seems generally plausible, as all KvS subunits imbue kinetics and voltage dependencies distinct from Kv2 (Bocksteins, 2016). For example, Kv6.4 alters the voltage-activation of Kv2.1 subunits (Bocksteins et al., 2017), and alters dynamics of the S6 pore-gating apparatus (Pisupati et al., 2018). Notably, the S6 helical bundle crossing of Kv2.1 constricts asymmetrically during channel inactivation in ways that are allosterically modulated by 4-aminopyridine (Fernández-Mariño et al., 2023), and KvS-containing channels allosterically alter interactions with 4-aminopyridine (Stas et al., 2015). These observations suggest KvS subunits could allosterically disrupt RY785 inhibition.

While we have identified a potential means to isolate KvS conductances, it is important to consider the limitations of these findings.

First, although every KvS subunit we tested is resistant to RY785, and these subunits span all the KvS subfamilies (Kv5, Kv6, Kv8, and Kv9), we have not tested all KvS subunits, species variants, cell types, or voltage regimens. Any of these could alter the RY785 IC_{50}. Pharmacology can yield surprises, such as the unexpected resistance of human Nav1.7 to saxitoxin (Walker et al., 2012). The degree of resistance to RY785 may vary among KvS subunits as with other central cavity drugs such as tetraethylammonium and 4-aminopyridine (Post et al., 1996; Thorneloe and Nelson, 2003; Stas et al., 2015). While Kv2.1/Kv8.1 channels appeared to be homogenously susceptible to RY785 (with Hill slope close to 1), other KvS subunits might present multiple pharmacologically-distinct heteromer populations.

Second, it is possible that RY785 can modulate other voltage-gated channels. However, we think

RY785 is unlikely to have substantial off-target effects as RY785 is much less potent against other non-Kv2 voltage-gated potassium channel subtypes as well as voltage-gated sodium and calcium channels (Herrington et al., 2011).

Third, concentrations of RY785 which partially blocked Kv2.1/Kv8.1 modified the gating of the voltage-activated conductance, indicating that RY785 can alter properties of heteromer conductance. Notably, 4-aminopyridine can increase Kv2 or Kv2/KvS conductances under specialized conditions (Stas et al., 2015; Fernández-Mariño et al., 2023). As discussed above, channel state-dependent binding is expected to influence the affinity of RY785.

Fourth, it is possible that other factors could imbue RY785 resistance. While it seems unlikely that pore-forming subunits other than KvS subunits complex with Kv2 subunits, other factors could potentially disrupt the RY785 site. Regulation of Kv2 channel gating could potentially allosterically disrupt RY785 inhibition. Extensive homeostatic regulation of Kv2.1 gating maintains neuronal excitability (Misonou et al., 2006); for example, ischemia (Misonou et al., 2005; Aras et al., 2009), glutamate (Misonou et al., 2008), phosphorylation (Murakoshi et al., 1997), SUMOylation (Plant et al., 2011) and AMIGO auxiliary subunits (Peltola et al., 2011; Maverick et al., 2021) all alter Kv2 gating.

Despite these possibilities, we think the most parsimonious interpretation of RY785-resistant, GxTX-sensitive conductances is that they are produced by heterotetrameric Kv2/KvS channels. However, it is important to consider other possibilities when interpreting RY785 resistance of GxTX-sensitive conductances. With these caveats in mind, we suggest that RY785-resistance combined with GxTX-sensitivity is strong evidence for Kv2/KvS channel currents.

Delayed-rectifier Kv2-like conductances are prominent in many electrically excitable cell types. Our findings in *Mrgprd*-lineage mouse DRG neurons as well as human DRG neurons suggest that the majority of the Kv2 conductance originates from Kv2/KvS channels, while in mouse SCG neurons Kv2-only channels seem to predominate. Beyond these cell types, it is unclear how prevalent KvS-containing conductances are. While Kv2 subunits are broadly expressed in electrically excitable cells throughout the brain and body, transcripts for KvS subunits have unique expression patterns that are specific to each KvS family member (Bocksteins, 2016) which can fluctuate with age (Regnier et al., 2016). However, transcript levels alone are not sufficient to predict protein levels (Liu et al., 2016). We found recently that native Kv2 channels in mouse brain contain KvS subunits, including Kv5.1, Kv8.1. Kv9.1 and Kv9.2. Notably, the KvS mass spectral abundance relative to Kv2.1 ranged from ≈18% for Kv5.1 to 2% for Kv9.1 (Ferns et al., 2024), and Kv5.1 protein expression was largely restricted to cortical neurons. Thus, it seems likely that significant KvS conductances also exist in specific subsets of brain neurons.

The physiological role of Kv2/KvS channels in neurons and other excitable cells remains enigmatic. Previous studies have used knockout mice (Regnier et al., 2017; Miyamae et al., 2021), transient transfection of KvS subunits (Lee et al., 2020b), siRNA knockdown (Tsantoulas et al., 2012), and modeling (Miyamae et al., 2021) to probe the presence of endogenous and functional KvS-containing channels, and these methods can identify phenotypic changes that suggest potential roles of KvS-containing channels. Moreover, genetic mutations and gene targeting studies have linked disruptions in the function of KvS-containing channels to epilepsy (Jorge et al., 2011), neuropathic pain sensitivity (Tsantoulas et al., 2018), labor pain (Lee et al., 2020a) and retinal cone dystrophy (Wu et al., 2006; Hart et al., 2019; Inamdar et al., 2022), stressing their functional importance in specific cell types. The unique pharmacology of KvS-containing channels identified here provides a new and direct method of identifying conductances mediated by KvS-containing channels in native neurons, and establishing what contributions KvS subunits make to electrophysiological signaling.

Finally, these findings also support the potential utility of KvS channels as drug targets. Kv2-targeted drug leads have poor tissue and cell specificity and suffer from pronounced side effects (Li et al., 2013).

KvS transcripts show far greater tissue- and cell-type specific expression relative to Kv2 (Bishop et al., 2015; Bocksteins, 2016), and we identified prominent KvS conductances in mouse nociceptor and human DRG neurons. Consequently, KvS-targeted drugs could offer greater specificity and the ability to modulate neuronal excitability in a variety of pathological contexts, such as neuropathic pain.

MATERIALS AND METHODS

- Mice

Studies were approved by the UC Davis and Harvard Medical School Institutional Animal Care and Use Committees and conform to guidelines established by the NIH. Mice were maintained on a 12 hr light/dark cycle, and food and water were provided ad libitum. The *Mrgprd*^{GFP} mouse line was a generous gift from David Ginty at Harvard (MGI: 3521853).

- Human tissue collection

Human dorsal root ganglia (DRG) were obtained from Sierra Donor Services. The donor was a 58-year-old Asian Indian female and DRG were from the 1st and 2nd lumbar region (cause of death: Stroke). DRG were extracted 6 hours after aortic cross clamp and placed in an ice cold N-methyl-D-glucamine-artificial cerebral spinal fluid (NMDG-aCSF) solution containing in mM: 93 NMDG, 2.5 KCl, 1.25 NaH_2PO_4, 30 $NaHCO_3$, 20 HEPES, 25 Glucose, 5 L-Ascorbic acid, 2 Thiourea, 3 Na pyruvate, 10 $MgSO_4$ and 0.5 $CaCl_2$ pH adjusted to 7.4 with HCl. Human DRG were obtained from the organ donor with full legal consent for use of tissue for research in compliance with procedures approved by Sierra Donor Services.

- Chinese hamster ovary (CHO) cell culture and transfection

The CHO-K1 cell line transfected with a tetracycline-inducible rat Kv2.1 construct (Kv2.1-CHO; Trapani and Korn, 2003) was cultured as described previously (Tilley et al., 2014). Transfections were achieved with Lipofectamine 3000 (Life Technologies, L3000001). 1 µl Lipofectamine was diluted, mixed, and incubated in 25 µl of Opti-MEM (Gibco, 31985062). Concurrently, 0.5 µg of KvS or AMIGO1 or Navβ2, 0.5 µg of pEGFP, 2 µl of P3000 reagent and 25 µl of Opti-MEM were mixed. DNA and Lipofectamine 3000 mixtures were mixed and incubated at room temperature for 15 min. This transfection cocktail was added to 1 ml of culture media in a 24 well cell culture dish containing Kv2.1-CHO cells and incubated at 37 °C in 5% CO_2 for 6 h before the media was replaced. Immediately after media was replaced, Kv2.1 expression was induced in Kv2.1-CHO cells with 1 µg/ml minocycline (Enzo Life Sciences, ALX-380-109-M050), prepared in 70% ethanol at 2 mg/ml. Voltage clamp recordings were performed 12-24 hours later. During recordings, the experimenter was blinded as to whether cells had been transfected with KvS, or Navβ2 or AMIGO1. Human Kv5.1, human Kv6.4 and human Kv8.1, AMIGO1-YFP, and pEGFP plasmids were gifts from James Trimmer (University of California, Davis, Davis, CA). Human Kv9.1 and human Kv9.3 plasmids were purchased from Addgene. Human Navβ2 plasmid was a kind gift from Dr. Alfred George (Lossin et al., 2002).

- Neuron cell culture

  - Mouse

Cervical, thoracic and lumbar dorsal root ganglia (DRGs) were harvested from 7- to 10-week-old *Mrgprd*^{GFP} mice and transferred to Hank's buffered saline solution (HBSS) (Invitrogen). Ganglia were treated with collagenase (2 mg/ml; Type P, Sigma-Aldrich) in HBSS for 15 min at 37 °C followed by 0.05% Trypsin-EDTA (Gibco) for 2.5 min with gentle rotation. Trypsin was neutralized with culture media (MEM, with l-glutamine, Phenol Red, without sodium pyruvate) supplemented with 10% horse serum (heat-inactivated; Gibco), 10 U/ml penicillin, 10 µg/ml streptomycin, MEM vitamin solution (Gibco), and B-27 supplement (Gibco). Serum-containing media was decanted and cells were triturated using a fire-polished Pasteur pipette in MEM culture media containing the supplements listed above. Cells were

plated on laminin-treated (0.05 mg/ml, Sigma-Aldrich) 5 mm German glass coverslips (Bellco Glass, 1943-00005), which had previously been washed in 70% ethanol and sterilized with ultraviolet light. Cells were then incubated at 37 °C in 5% CO_2. Cells were used for electrophysiological experiments 24–38 hr after plating.

Superior cervical ganglia (SCG) were harvested from Swiss Webster (CFW) mice (postnatal day 13-15, either sex) and treated for 20 min at room temperature (RT) with 20 U/ml papain (Worthington Biochemical), 5 mM dl-cysteine, 1.25 mM EDTA, and 67 μM β-mercaptoethanol in a Ca^{2+}, Mg^{2+}-free (CMF) Hank's solution (Gibco) supplemented with 1 mM Sodium Pyruvate (Sigma-Aldrich, St. Louis, MO), and 5 mM HEPES (Sigma-Aldrich, St. Louis, MO). Ganglia were then treated for 20 min at 37 °C with 3 mg/ml collagenase (type I; Roche Diagnostics) and 3 mg/ml dispase II (Roche Diagnostics) in CMF Hank's solution. Cells were dispersed by trituration with fire-polished Pasteur pipettes in a solution composed of two media combined in a 1:1 ratio: Leibovitz's L-15 (Invitrogen) supplemented with 5 mM HEPES, and DMEM/F12 medium (Invitrogen). Cells were then plated on glass coverslips and incubated at 37 °C (95% O_2, 5% CO_2) for 1 hr, after which Neurobasal medium (Invitrogen) with B-27 supplement (Invitrogen), penicillin and streptomycin (Sigma) was added to the dish. Cells were incubated at 25 °C (95% O_2, 5% CO_2) and used within 10 hr.

- Human

Dura were removed from human DRG with a scalpel in ice cold NMDG-aCSF solution (Valtcheva et al., 2016). Human DRG were then cut into approximately 1 mm thick sections and were placed in 1.7 mg/mL Stemxyme (Worthington Biochemical, LS004107) and 6.7 mg/mL DNAse I (Worthington Biochemical, LSOO2139) diluted in HBSS (Thermo Fisher Scientific, 14170161) for 12 hr at 37 °C. DRG were then triturated with a fire-polished Pasteur pipette and passed through a 100 µm cell strainer. Cells were then spun at 900 g through 10% BSA. The supernatant was removed, and cells were resuspended in human DRG culturing media that contained 1% penicillin/streptomycin, 1% GlutaMAX (Gibco, 35050-061), 2% NeuroCult SM1 (05711, Stemcell technologies), 1% N2 Supplement (Thermo Scientific, 17502048), 2% FBS (Gibco, 26140-079) diluted in BrainPhys media (Stemcell tehnologies, 05790). DRG neurons were plated on poly-D-lysine treated (0.01 mg/mL) 5 mm German glass coverslips, which had previously been washed in 70% ethanol and sterilized with ultraviolet light. DRG neurons were then incubated at 37 °C in 5% CO_2. Human DRG neuron experiments were performed up to 7 days after plating.

- Whole cell voltage clamp of CHO cells

Voltage clamp was achieved with a dPatch amplifier (Sutter Instruments) run by SutterPatch software (Sutter Instruments). Solutions for Kv2.1-CHO cell voltage-clamp recordings: CHO-internal (in mM) 120 K-methylsulfonate, 10 KCl, 10 NaCl, 5 EGTA, 0.5 CaCl2, 10 HEPES, 2.5 MgATP pH adjusted to 7.2 with KOH, 289 mOsm. CHO-external (in mM) 145 NaCl, 5 KCl, 2 CaCl2, 2 MgCl2, 10 HEPES pH adjusted to 7.3 with NaOH, 298 mOsm. Osmolality was measured with a vapor pressure osmometer (Wescor, 5520). The liquid junction potential of -9 mV between these solutions was accounted for. The liquid junction potential was calculated according to the stationary Nernst–Planck equation (Marino. et al., 2014) using LJPcalc (RRID:SCR_025044). For voltage-clamp recordings, Kv2.1-CHO cells were detached in a PBS-EDTA solution (Gibco, 15040-066), spun at 500 g for 2 minutes and then resuspended in 50% cell culture media and 50% CHO-external recording solution. Cells were then added to a recording chamber (Warner, 64–0381) and were rinsed with the CHO-external patching solution after adhering to the bottom of the recording chamber. Transfected Kv2.1-CHO cells were identified by GFP fluorescence and were selected for whole cell voltage clamp. Thin-wall borosilicate glass recording pipettes (Sutter,

BF150-110-10) were pulled with blunt tips, coated with silicone elastomer (Sylgard 184, Dow Corning), heat cured, and tip fire-polished to resistances less than 4 MΩ. Series resistance of 2–14 MΩ was estimated from the Sutterpatch whole-cell parameters routine. Series resistance compensation between 13 and 90% was used to constrain voltage error to less than 15 mV; compensation feedback lag was 6 µs for most experiments or 100 µs for concentration-effect experiments. Capacitance and ohmic leak were subtracted using a P/4 protocol. Output was low-pass filtered at 5 kHz using the amplifier's built-in Bessel and digitized at 25 kHz or, for concentration-effect experiments, 1 and 10 kHz. Experiments were performed on Kv2.1-CHO cells with membrane resistance greater than 1 GΩ assessed prior to running voltage clamp protocols while cells were held at a membrane potential of –89 mV. RY785 (gift from Bruce Bean, Harvard, or Cayman, 19813) was prepared in DMSO as a 1 mM stock for dilutions to 1 µM or a 35 mM stock for concentration-effect experiments. Stocks of GxTX-1E Met35Nle (Tilley et al., 2014) in water were 10 µM. Stocks were stored frozen and diluted in recording solution just prior to application to cells. Solutions were flushed over cells at a rate of approximately 1 mL/min. Concentrated RY785 and GxTX stocks were stored at -20 °C. Kv2.1-CHO cells were given voltage steps from -89 mV to -9 mV for 200 ms every 6 seconds during application of RY785 until currents stabilized. When vehicle control was applied to cells, -9 mV steps were given for a similar duration. The DMSO concentration in RY785 and vehicle control solutions was 0.1%. Perfusion lines were cleaned with 70% ethanol then doubly-deionized water. For concentration-effect experiments, changes in current amplitude due to solution exchange were controlled for by treating every other tested cell with multiple washes of the same, 0.35 µM RY785 solution instead of increasing concentrations of RY785. The timing and duration of these control washes was similar to that of the washes in concentration-effect experiments.

- Whole cell voltage clamp of mouse and human dorsal root ganglion neurons

Whole cell recordings from mouse and human neurons were performed using the same methods as CHO cell recordings with the following exceptions. Voltage clamp was achieved with a dPatch amplifier run by SutterPatch software or an AxoPatch 200B amplifier (Molecular Devices) controlled by PatchMaster software (v2x91, HEKA Elektronik) via an ITC-18 A/D board (HEKA Instruments Inc). Solutions for voltage-clamp recordings: internal (in mM) 140 KCl, 13.5 NaCl, 1.8 $MgCl_2$ 0.09 EGTA, 4 MgATP, 0.3 Na_2GTP, 9 HEPES pH adjusted to 7.2 with KOH, 326 mOsm. The external solution contained (in mM) 3.5 KCl, 155 NaCl, 1 $MgCl_2$, 1.5 $CaCl_2$, 0.01 $CdCl_2$, 10 HEPES, 10 glucose pH adjusted to 7.4 with NaOH, 325 mOsm. The calculated liquid junction potential of -4 mV between these solutions was accounted for. For voltage-clamp recordings, neurons on cover slips were placed in the same recording chamber used for CHO cell recordings and were rinsed with an external patching solution. Neurons from *Mrgprd*^{GFP} mice with green fluorescence were selected for recordings. Human DRG neurons with cell capacitances between 22.5 and 60 pF were used. After whole-cell voltage clamp was established, Kv2/KvS conductances were isolated by exchanging the external solution with external solution containing 100 nM alpha-dendrotoxin (Alomone) to block Kv1, 3 µM AmmTX3 (Alomone) to block Kv4, 100 µM 4-aminopyridine to block Kv3, 1 µM TTX to block TTX sensitive Nav channels, and 10 µM A-803467 (Tocris) to block Nav1.8. After addition of 1 µM RY785 neurons were given 10 steps to -24 mV for 500 ms to allow for voltage dependent block of RY785. Thin-wall borosilicate glass recording pipettes were pulled with blunt tips, coated with silicone elastomer, heat cured, and tip fire-polished to resistances less than 2 MΩ. Series resistance of 1–4 MΩ was estimated from the whole-cell parameters circuit. Series resistance compensation between 55 and 98% was used to constrain voltage error to less than 15 mV. Ohmic leak was not subtracted. Neurons were held at a membrane potential of –74 mV.

- Whole cell voltage clamp of mouse superior cervical ganglion neurons

Whole cell recordings from mouse superior cervical ganglion neurons were performed using an Axon Instruments Multiclamp 700B Amplifier (Molecular Devices). Electrodes were pulled on a Sutter P-97 puller (Sutter Instruments) and shanks were wrapped with Parafilm (American National Can Company) to allow optimal series resistance compensation without oscillation. Voltage or current commands were delivered and signals were recorded using a Digidata 1321A data acquisition system (Molecular Devices) controlled by pCLAMP 9.2 software (Molecular Devices). The internal solution was (in mM): 140 mM K aspartate, 13.5 mM NaCl, 1.8 mM MgCl2, 0.09 mM EGTA, 9 mM HEPES, 14 mM creatine phosphate (Tris salt), 4 mM MgATP, 0.3 mM Tris-GTP, pH 7.2 adjusted with KOH. The base external solution was the same as for DRG recordings: (in mM) 3.5 KCl, 155 NaCl, 1 MgCl2, 1.5 CaCl2, and 0.01 CdCl2, 10 HEPES 10 glucose pH adjusted to 7.4 with NaOH, 325 mOsm. The calculated liquid junction potential of -15 mV between these solutions was accounted for. After establishing whole-cell recording, cell capacitance was nulled and series resistance was partially (60%) compensated to constrain voltage error to less than 2 mV. The cell was then lifted and placed in front of a series of quartz fiber flow pipes for rapid solution exchange and application of RY785 and GxTX. The external solution used for recording Kv2 currents used the same cocktail of inhibitors for sodium channels and other potassium channels as for the DRG recordings except that A-803467 was omitted because the sodium current in SCG neurons is all TTX sensitive (Toledo-Aral et al., 1997): 100 nM alpha-dendrotoxin (Alomone), 1 µM TTX, 3 µM AmmTX3 (Alomone), and 100 µM 4-aminopyridine.

- Voltage clamp analysis

Activation kinetics were fit from 10-90% of current (I_K) rise with the power of an exponential function:

Equation 1

$$I_K = A\left(1 - e^{\frac{-t}{\tau_{act}}}\right)^{\sigma}$$

where A is the maximum current amplitude, $\tau_{act}$is the time constant of activation, σ is sigmoidicity, and t is time. The t = 0 mark was adjusted to 100 µs after the start of the voltage step from the holding potential to correct for filter delay and cell charging.

Conductance values were determined from tail current levels at -9 mV after 200 ms steps to the indicated voltage. Tail currents were the mean current amplitude from 1 to 5 ms into the -9 mV step. Conductance–voltage relations were fit with the Boltzmann function:

Equation 2

$$f(V) = A\left(1 + e^{-\left(V - V_{\frac{1}{2}}\right)\frac{zF}{RT}}\right)^{-1}$$

where V is voltage, A is amplitude, z is the number of elementary charges, F is Faraday's constant, R is the universal gas constant, and T is temperature (held at 295 K).

Deactivation kinetics were fit with a double exponential:

Equation 3

$$f(x) = y_0 + A_1 e^{\frac{-(t-t_0)}{\tau_1}} + A_2 e^{\frac{-(t-t_0)}{\tau_2}}$$

Where t is time, y_0 is the initial current amplitude, t_0 is the start time of the exponential decay, τ_1 and τ_2 are the time constants, and A_1 and A_2 are the amplitudes of each component.

- Immunofluorescence

Kv2.1-CHO cells were fixed for 15 minutes at 4 °C in 4% formaldehyde prepared fresh from paraformaldehyde in PBS buffer pH 7.4. Cells were then washed 3 x 5 minutes in PBS, followed by blocking in blotto-PBS (PBS, pH 7.4 with 4% (w/v) non-fat milk powder and 0.1% (v/v) Triton-X100) for 1 hr. Cells were incubated for 1 hr with primary antibodies diluted in blotto-PBS and subsequently washed 3 x 5 minutes in PBS. Antibodies used were mAb K89/34 for Kv2.1 (NeuroMab, RRID:AB_1067225), rabbit pAb 5.1C for Kv5.1 (in-house, RRID:AB_3076240), and rabbit anti-V5 for Kv9.3-V5 (Rockland, 600-401-378). For surface labeling of Kv5.1, non-permeabilized cells were incubated with Kv5.1 mAb (Santa Cruz Biotech, 81881) in blotto-PBS lacking Triton-X100. The cells were then incubated with mouse IgG subclass- and/or species-specific Alexa-conjugated fluorescent secondary antibodies (Invitrogen) diluted in blotto-PBS for 45 min and washed 3 x 5 min in PBS. Cover glasses were mounted on microscope slides with Prolong Gold mounting medium (ThermoFisher, P36930) according to the manufacturer's instructions. Widefield fluorescence images were acquired with an AxioCam MRm digital camera installed on a Zeiss AxioImager M2 microscope with a 63×/1.40 NA Plan-Apochromat oil immersion objective and an ApoTome coupled to Axiovision software version 4.8.2.0 (Zeiss, Oberkochen, Germany).

- Multiplex in situ hybridization

A 6-week-old *Mrgprd*^{GFP} mouse was briefly anesthetized with 3–5% isoflurane and then decapitated. The spinal column was dissected, and the left and right L1 DRG were removed and drop fixed for 12 minutes in ice cold 4% paraformaldehyde in 0.1 M phosphate buffer (PB) pH adjusted to 7.4. The L1 vertebrae was identified by the 13th rib. The DRG was washed 3 × 10 minutes each in PB and cryoprotected at 4 °C in 30% sucrose diluted in PB for 2 hr. The DRG were then frozen in Optimal Cutting Temperature (OCT) compound (Fisher, 4585) and stored at –80 °C until sectioning. Samples were cut into 20 µm sections on a freezing stage sliding microtome and were collected on Colorfrost Plus microscope slides (Fisher Scientific, 12-550-19). Sections were processed for RNA *in situ* detection using an RNAscope Fluorescent Detection Kit according to the manufacturer's instructions (Advanced Cell Diagnostics) with the following probes: *KCNF1* (508731, mouse) or *KCNS1* (525941, mouse). TSA Vivid 650 Fluorophore was used to label probes (TSA Vivid, 7527) Following in situ hybridization, immunohistochemistry to label GFP was performed. Sections were incubated in vehicle solution (4% milk, 0.2% triton diluted in PB) for 1 hr at RT. Tissue was then incubated in a rabbit polyclonal anti-GFP antibody (Rockland 600-401-215S) diluted 1:1000 in vehicle overnight at 4 °C. Sections were washed three times in vehicle for 5 minutes per wash and then incubated in a goat anti-rabbit secondary antibody (Invitrogen, A-11008) diluted 1:1500 in vehicle. Sections were then mounted with Prolong Gold (Thermo Fisher, P36930) and #1.5 cover glass (Fisher Scientific, NC1776158).

- Imaging

Images were acquired with an inverted scanning confocal and airy disk imaging system (Zeiss LSM 880 Airyscan, 410900-247-075) run by ZEN black v2.1. Laser lines were 488 nm and 633 nm. Images were acquired with a 0.8 NA 20x objective (Zeiss, 420650-9901) details in figure legends.

- Statistics

All statistical tests were performed in Igor Pro software version 8 (Wavemetrics, Lake Oswego, OR). Independent replicates (n) are individual cells/neurons while biological replicates (N) are individual mice. All tests were two-tailed. Wilcoxon rank tests were used for two-sample comparisons. Dunnett tests were used for multiple comparisons.

ACKNOWLEDGMENTS

We thank the human tissue donors and their families for their generous donations. We thank Sierra Donor Services for recovering human dorsal root ganglia, as well as Sean Van Slyck, Marnae Salampessy, and Theanne Griffith for helping arrange for human tissue. We thank Bryan Copits, Ted Price, and Juliet Mwirigi for advice on culturing human neurons. We thank Cyrrus Espino, Hai Nguyen, and Geir Hareland for preparation of human tissues. We thank Josh Tulman for illustrations. We thank Bruce Bean for scientific discussions and feedback on the manuscript. GxTx-Nle35 was synthesized at the Molecular Foundry of the Lawrence Berkeley National Laboratory under U.S. Department of Energy contract DE-AC02-05CH11231. Research at the University of California Davis was supported by the University of California Davis and U.S. National Institutes of Health grant R03-TR004200. Research at Harvard was supported by National Institutes of Health grant R35-NS127216. The Neurobiology Course at the Marine Biological Laboratory is supported by National Institutes of Health grant R25-NS063307.

REFERENCES

Aras MA, Saadi RA, Aizenman E (2009) Zn2+ regulates Kv2.1 voltage-dependent gating and localization following ischemia. Eur J Neurosci 30:2250-2257.

Bishop HI, Guan D, Bocksteins E, Parajuli LK, Murray KD, Cobb MM, Misonou H, Zito K, Foehring RC, Trimmer JS (2015) Distinct cell- and layer-specific expression patterns and independent regulation of Kv2 channel subtypes in cortical pyramidal neurons. J Neurosci 35:14922-14942.

Bocksteins E (2016) Kv5, Kv6, Kv8, and Kv9 subunits: No simple silent bystanders. J Gen Physiol 147:105-125.

Bocksteins E, Snyders DJ (2012) Electrically silent Kv subunits: their molecular and functional characteristics. Physiology (Bethesda) 27:73-84.

Bocksteins E, Snyders DJ, Holmgren M (2017) Independent movement of the voltage sensors in K(V)2.1/K(V)6.4 heterotetramers. Sci Rep 7:41646.

Bocksteins E, Labro AJ, Snyders DJ, Mohapatra DP (2012) The electrically silent Kv6.4 subunit confers hyperpolarized gating charge movement in Kv2.1/Kv6.4 heterotetrameric channels. PLoS One 7:e37143.

Bocksteins E, Raes AL, Van de Vijver G, Bruyns T, Van Bogaert PP, Snyders DJ (2009) Kv2.1 and silent Kv subunits underlie the delayed rectifier K+ current in cultured small mouse DRG neurons. Am J Physiol Cell Physiol 296:C1271-1278.

Castellano A, Chiara MD, Mellstrom B, Molina A, Monje F, Naranjo JR, Lopez-Barneo J (1997) Identification and functional characterization of a K+ channel alpha-subunit with regulatory properties specific to brain. J Neurosci 17:4652-4661.

Du J, Haak LL, Phillips-Tansey E, Russell JT, McBain CJ (2000) Frequency-dependent regulation of rat hippocampal somato-dendritic excitability by the K+ channel subunit Kv2.1. J Physiol 522 Pt 1:19-31.

Fernández-Mariño AI, Tan XF, Bae C, Huffer K, Jiang J, Swartz KJ (2023) Inactivation of the Kv2.1 channel through electromechanical coupling. Nature 622:410-417.

Ferns M, Van der List D, Vierra NC, Lacey T, Murray KD, Kirmiz M, Stewart RG, Sack JT, Trimmer JS (2024) Electrically silent KvS subunits associate with native Kv2 channels in brain and impact diverse properties of channel function. bioRxiv:2024.2001.2025.577135.

Hart NS, Mountford JK, Voigt V, Fuller-Carter P, Barth M, Nerbonne JM, Hunt DM, Carvalho LS (2019) The Role of the Voltage-Gated Potassium Channel Proteins Kv8.2 and Kv2.1 in Vision and Retinal Disease: Insights from the Study of Mouse Gene Knock-Out Mutations. eNeuro 6:ENEURO.0032-0019.2019.

Herrington J, Solly K, Ratliff KS, Li N, Zhou YP, Howard A, Kiss L, Garcia ML, McManus OB, Deng Q, Desai R, Xiong Y, Kaczorowski GJ (2011) Identification of novel and selective Kv2 channel inhibitors. Mol Pharmacol 80:959-964.

Herrington J et al. (2006) Blockers of the delayed-rectifier potassium current in pancreatic beta-cells enhance glucose-dependent insulin secretion. Diabetes 55:1034-1042.

Inamdar SM, Lankford CK, Poria D, Laird JG, Solessio E, Kefalov VJ, Baker SA (2022) Differential impact of Kv8.2 loss on rod and cone signaling and degeneration. Hum Mol Genet 31:1035-1050.

Johnson B, Leek AN, Sole L, Maverick EE, Levine TP, Tamkun MM (2018) Kv2 potassium channels form endoplasmic reticulum/plasma membrane junctions via interaction with VAPA and VAPB. Proc Natl Acad Sci U S A 115:E7331-e7340.

Jorge BS, Campbell CM, Miller AR, Rutter ED, Gurnett CA, Vanoye CG, George AL, Jr., Kearney JA (2011) Voltage-gated potassium channel KCNV2 (Kv8.2) contributes to epilepsy susceptibility. Proc Natl Acad Sci U S A 108:5443-5448.

Kerschensteiner D, Stocker M (1999) Heteromeric assembly of Kv2.1 with Kv9.3: effect on the state dependence of inactivation. Biophys J 77:248-257.
Kerschensteiner D, Soto F, Stocker M (2005) Fluorescence measurements reveal stoichiometry of K+ channels formed by modulatory and delayed rectifier alpha-subunits. Proc Natl Acad Sci U S A 102:6160-6165.
Kirmiz M, Palacio S, Thapa P, King AN, Sack JT, Trimmer JS (2018) Remodeling neuronal ER-PM junctions is a conserved nonconducting function of Kv2 plasma membrane ion channels. Mol Biol Cell:mbcE18050337.
Kobertz WR (2018) Oddballs in the Shaker family: Kv2-related regulatory subunits. J Gen Physiol 150:1599-1601.
Kramer JW, Post MA, Brown AM, Kirsch GE (1998) Modulation of potassium channel gating by coexpression of Kv2.1 with regulatory Kv5.1 or Kv6.1 alpha-subunits. Am J Physiol 274:C1501-1510.
Lee MC, Nahorski MS, Hockley JRF, Lu VB, Ison G, Pattison LA, Callejo G, Stouffer K, Fletcher E, Brown C, Drissi I, Wheeler D, Ernfors P, Menon D, Reimann F, Smith ESJ, Woods CG (2020a) Human Labor Pain Is Influenced by the Voltage-Gated Potassium Channel K(V)6.4 Subunit. Cell Rep 32:107941.
Lee MC, Nahorski MS, Hockley JRF, Lu VB, Ison G, Pattison LA, Callejo G, Stouffer K, Fletcher E, Brown C, Drissi I, Wheeler D, Ernfors P, Menon D, Reimann F, Smith ESJ, Woods CG (2020b) Human labor pain is influenced by the voltage-gated potassium channel Kv 6.4 subunit. Cell Rep 32:107941.
Li XN, Herrington J, Petrov A, Ge L, Eiermann G, Xiong Y, Jensen MV, Hohmeier HE, Newgard CB, Garcia ML, Wagner M, Zhang BB, Thornberry NA, Howard AD, Kaczorowski GJ, Zhou YP (2013) The role of voltage-gated potassium channels Kv2.1 and Kv2.2 in the regulation of insulin and somatostatin release from pancreatic islets. J Pharmacol Exp Ther 344:407-416.
Liu PW, Bean BP (2014) Kv2 channel regulation of action potential repolarization and firing patterns in superior cervical ganglion neurons and hippocampal CA1 pyramidal neurons. J Neurosci 34:4991-5002.
Liu Y, Beyer A, Aebersold R (2016) On the Dependency of Cellular Protein Levels on mRNA Abundance. Cell 165:535-550.
Lossin C, Wang DW, Rhodes TH, Vanoye CG, George AL, Jr. (2002) Molecular basis of an inherited epilepsy. Neuron 34:877-884.
Marino. M, Misuri. L, Brogioli. D (2014) A new open source software for the calculation of the liquid junction potential between two solutions according to the stationary Nernst-Planck equation. arXiv:14033640.
Marquis MJ, Sack JT (2022) Mechanism of use-dependent Kv2 channel inhibition by RY785. J Gen Physiol 154:e202112981.
Matsumoto C, O'Dwyer SC, Manning D, Hernandez-Hernandez G, Rhana P, Fong Z, Sato D, Clancy CE, Vierra NC, Trimmer JS, Fernando Santana L (2023) The formation of K(V)2.1 macro-clusters is required for sex-specific differences in L-type Ca(V)1.2 clustering and function in arterial myocytes. Commun Biol 6:1165.
Maverick EE, Leek AN, Tamkun MM (2021) Kv2 channel-AMIGO β-subunit assembly modulates both channel function and cell adhesion molecule surface trafficking. J Cell Sci 134.
Milescu M, Lee HC, Bae CH, Kim JI, Swartz KJ (2013) Opening the shaker K+ channel with hanatoxin. J Gen Physiol 141:203-216.
Milescu M, Bosmans F, Lee S, Alabi AA, Kim JI, Swartz KJ (2009) Interactions between lipids and voltage sensor paddles detected with tarantula toxins. Nat Struct Mol Biol 16:1080-1085.
Misonou H, Thompson SM, Cai X (2008) Dynamic regulation of the Kv2.1 voltage-gated potassium channel during brain ischemia through neuroglial interaction. J Neurosci 28:8529-8538.

Misonou H, Mohapatra DP, Menegola M, Trimmer JS (2005) Calcium- and metabolic state-dependent modulation of the voltage-dependent Kv2.1 channel regulates neuronal excitability in response to ischemia. J Neurosci 25:11184-11193.
Misonou H, Menegola M, Mohapatra DP, Guy LK, Park KS, Trimmer JS (2006) Bidirectional activity-dependent regulation of neuronal ion channel phosphorylation. J Neurosci 26:13505-13514.
Miyamae T, Hashimoto T, Abraham M, Kawabata R, Koshikizawa S, Bian Y, Nishihata Y, Kikuchi M, Ermentrout GB, Lewis DA, Gonzalez-Burgos G (2021) Kcns3 deficiency disrupts Parvalbumin neuron physiology in mouse prefrontal cortex: Implications for the pathophysiology of schizophrenia. Neurobiol Dis 155:105382.
Moller L, Regnier G, Labro AJ, Blunck R, Snyders DJ (2020) Determining the correct stoichiometry of Kv2.1/Kv6.4 heterotetramers, functional in multiple stoichiometrical configurations. Proc Natl Acad Sci U S A 117:9365-9376.
Murakoshi H, Shi G, Scannevin RH, Trimmer JS (1997) Phosphorylation of the Kv2.1 K+ channel alters voltage-dependent activation. Mol Pharmacol 52:821-828.
Peltola MA, Kuja-Panula J, Lauri SE, Taira T, Rauvala H (2011) AMIGO is an auxiliary subunit of the Kv2.1 potassium channel. EMBO Rep 12:1293-1299.
Pisupati A, Mickolajczyk KJ, Horton W, van Rossum DB, Anishkin A, Chintapalli SV, Li X, Chu-Luo J, Busey G, Hancock WO, Jegla T (2018) The S6 gate in regulatory Kv6 subunits restricts heteromeric K. J Gen Physiol 150:1702-1721.
Plant LD, Dowdell EJ, Dementieva IS, Marks JD, Goldstein SA (2011) SUMO modification of cell surface Kv2.1 potassium channels regulates the activity of rat hippocampal neurons. J Gen Physiol 137:441-454.
Post MA, Kirsch GE, Brown AM (1996) Kv2.1 and electrically silent Kv6.1 potassium channel subunits combine and express a novel current. FEBS Lett 399:177-182.
Ray P, Torck A, Quigley L, Wangzhou A, Neiman M, Rao C, Lam T, Kim JY, Kim TH, Zhang MQ, Dussor G, Price TJ (2018) Comparative transcriptome profiling of the human and mouse dorsal root ganglia: an RNA-seq-based resource for pain and sensory neuroscience research. Pain 159:1325-1345.
Regnier G, Bocksteins E, Van de Vijver G, Snyders DJ, van Bogaert PP (2016) The contribution of Kv2.2-mediated currents decreases during the postnatal development of mouse dorsal root ganglion neurons. Physiol Rep 4:e12731.
Regnier G, Bocksteins E, Marei WF, Pintelon I, Timmermans JP, Leroy JLMR, Snyders DJ (2017) Targeted deletion of the Kv6.4 subunit causes male sterility due to disturbed spermiogenesis. Reprod Fertil Dev 29:1567-1575.
Richardson FC, Kaczmarek LK (2000) Modification of delayed rectifier potassium currents by the Kv9.1 potassium channel subunit. Hear Res 147:21-30.
Salinas M, Duprat F, Heurteaux C, Hugnot JP, Lazdunski M (1997a) New modulatory alpha subunits for mammalian Shab K+ channels. The Journal of biological chemistry 272:24371-24379.
Salinas M, de Weille J, Guillemare E, Lazdunski M, Hugnot JP (1997b) Modes of regulation of shab K+ channel activity by the Kv8.1 subunit. J Biol Chem 272:8774-8780.
Sano Y, Mochizuki S, Miyake A, Kitada C, Inamura K, Yokoi H, Nozawa K, Matsushime H, Furuichi K (2002) Molecular cloning and characterization of Kv6.3, a novel modulatory subunit for voltage-gated K(+) channel Kv2.1. FEBS Lett 512:230-234.
Sapio MR, Vazquez FA, Loydpierson AJ, Maric D, Kim JJ, LaPaglia DM, Puhl HL, Lu VB, Ikeda SR, Mannes AJ, Iadarola MJ (2020) Comparative Analysis of Dorsal Root, Nodose and Sympathetic Ganglia for the Development of New Analgesics. Front Neurosci 14:615362.
Sepela RJ, Stewart RG, Valencia LA, Thapa P, Wang Z, Cohen BE, Sack JT (2022) The AMIGO1 adhesion protein activates Kv2.1 voltage sensors. Biophys J 121:1395-1416.

Stas JI, Bocksteins E, Labro AJ, Snyders DJ (2015) Modulation of Closed-State Inactivation in Kv2.1/Kv6.4 Heterotetramers as Mechanism for 4-AP Induced Potentiation. PLoS One 10:e0141349.
Stewart RG, Camacena M, Copits BA, Sack JT (2024) Distinct cellular expression and subcellular localization of Kv2 voltage-gated K(+) channel subtypes in dorsal root ganglion neurons conserved between mice and humans. J Comp Neurol 532:e25575.
Thapa P, Stewart R, Sepela RJ, Vivas O, Parajuli LK, Lillya M, Fletcher-Taylor S, Cohen BE, Zito K, Sack JT (2021) EVAP: A two-photon imaging tool to study conformational changes in endogenous Kv2 channels in live tissues. J Gen Physiol 153:e202012858.
Thorneloe KS, Nelson MT (2003) Properties and molecular basis of the mouse urinary bladder voltage-gated K+ current. J Physiol 549:65-74.
Tilley DC, Angueyra JM, Eum KS, Kim H, Chao LH, Peng AW, Sack JT (2019) The tarantula toxin GxTx detains K. J Gen Physiol 151:292-315.
Tilley DC, Eum KS, Fletcher-Taylor S, Austin DC, Dupré C, Patrón LA, Garcia RL, Lam K, Yarov-Yarovoy V, Cohen BE, Sack JT (2014) Chemoselective tarantula toxins report voltage activation of wild-type ion channels in live cells. Proc Natl Acad Sci U S A 111:E4789-E4796.
Toledo-Aral JJ, Moss BL, He ZJ, Koszowski AG, Whisenand T, Levinson SR, Wolf JJ, Silos-Santiago I, Halegoua S, Mandel G (1997) Identification of PN1, a predominant voltage-dependent sodium channel expressed principally in peripheral neurons. Proc Natl Acad Sci U S A 94:1527-1532.
Trimmer JS (1993) Expression of Kv2.1 delayed rectifier K+ channel isoforms in the developing rat brain. FEBS Lett 324:205-210.
Tsantoulas C, Denk F, Signore M, Nassar MA, Futai K, McMahon SB (2018) Mice lacking Kcns1 in peripheral neurons show increased basal and neuropathic pain sensitivity. Pain 159:1641-1651.
Tsantoulas C, Zhu L, Shaifta Y, Grist J, Ward JP, Raouf R, Michael GJ, McMahon SB (2012) Sensory neuron downregulation of the Kv9.1 potassium channel subunit mediates neuropathic pain following nerve injury. J Neurosci 32:17502-17513.
Valtcheva MV, Copits BA, Davidson S, Sheahan TD, Pullen MY, McCall JG, Dikranian K, Gereau RWt (2016) Surgical extraction of human dorsal root ganglia from organ donors and preparation of primary sensory neuron cultures. Nat Protoc 11:1877-1888.
Vierra NC, O'Dwyer SC, Matsumoto C, Santana LF, Trimmer JS (2021) Regulation of neuronal excitation-transcription coupling by Kv2.1-induced clustering of somatic L-type Ca(2+) channels at ER-PM junctions. Proc Natl Acad Sci U S A 118:e2110094118.
Walker JR, Novick PA, Parsons WH, McGregor M, Zablocki J, Pande VS, Du Bois J (2012) Marked difference in saxitoxin and tetrodotoxin affinity for the human nociceptive voltage-gated sodium channel (Nav1.7) [corrected]. Proc Natl Acad Sci U S A 109:18102-18107.
Wu H, Cowing JA, Michaelides M, Wilkie SE, Jeffery G, Jenkins SA, Mester V, Bird AC, Robson AG, Holder GE, Moore AT, Hunt DM, Webster AR (2006) Mutations in the gene KCNV2 encoding a voltage-gated potassium channel subunit cause "cone dystrophy with supernormal rod electroretinogram" in humans. Am J Hum Genet 79:574-579.
Zheng Y, Liu P, Bai L, Trimmer JS, Bean BP, Ginty DD (2019) Deep sequencing of somatosensory neurons reveals molecular determinants of intrinsic physiological properties. Neuron 103:598-616.e597.
Zhong XZ, Abd-Elrahman KS, Liao CH, El-Yazbi AF, Walsh EJ, Walsh MP, Cole WC (2010) Stromatoxin-sensitive, heteromultimeric Kv2.1/Kv9.3 channels contribute to myogenic control of cerebral arterial diameter. J Physiol 588:4519-4537.
Zylka MJ, Rice FL, Anderson DJ (2005) Topographically distinct epidermal nociceptive circuits revealed by axonal tracers targeted to Mrgprd. Neuron 45:17-25.

FIGURES AND LEGENDS

Figure 1

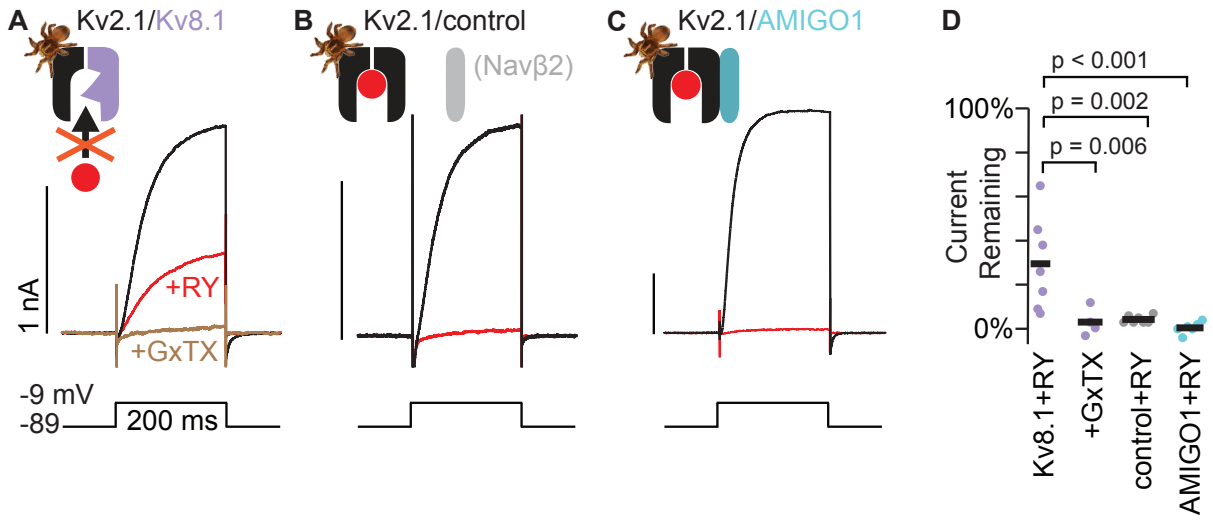

Figure 1. Kv2.1/Kv8.1 heteromers are resistant to RY785 and sensitive to GxTX

A) Exemplar traces from a voltage-clamped Kv2.1-CHO cell transfected with Kv8.1. Black and red traces are currents before and after application of 1 µM RY785 respectively. Brown trace is current after subsequent application of 1 µM RY785 and 100 nM GxTX.
B) Exemplar traces from a Kv2.1-CHO cell transfected with Navβ2.
C) Exemplar traces from a Kv2.1-CHO cell transfected with AMIGO1.
D) Current remaining after application of 1 µM RY785 or 1 µM RY785 + 100 nM GxTX. Black bars represent mean. Each point represents current from one cell at the end of a 200 ms voltage step to -9 mV. Dunnett tests with Kv8.1 + RY785 as control.

Figure 1 Supplement

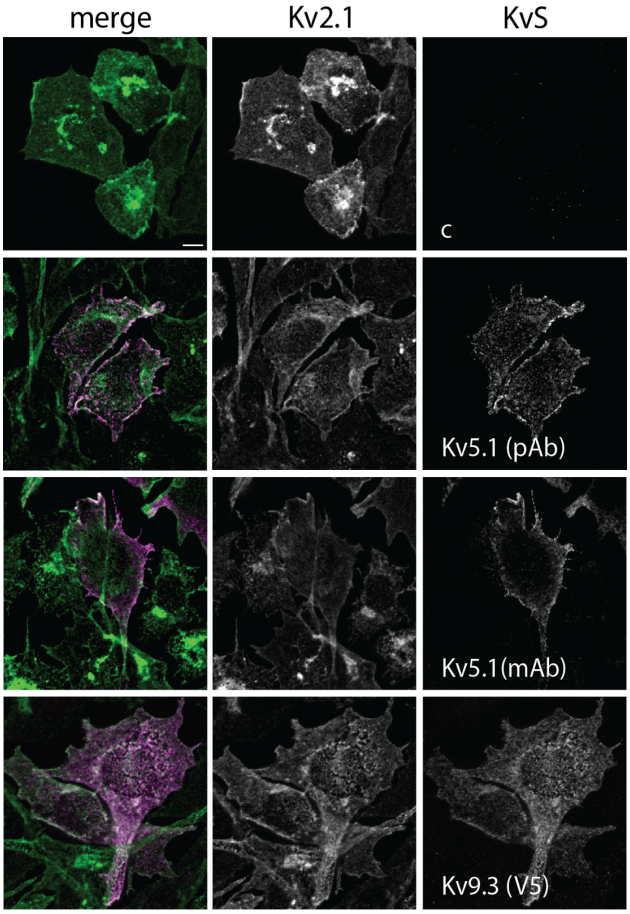

Figure 1 Supplement. KvS subunits colocalize with Kv2.1 on the surface of CHO cells.

Kv2.1-CHO cells transfected with the designated KvS subunits (c = no KvS transfection) were immunolabeled for Kv2.1 (green) and Kv5.1 or Kv9.3 (magenta). Immunolabeling for Kv5.1 and Kv9.3 were detected both intracellularly and on the apparent cell surface where they colocalized with Kv2.1 labeling. The anti-Kv5.1 mAb recognizes an extracellular epitope and was used on non-permeabilized cells, confirming surface expression of Kv5.1. Scale bars = 5 μm.

Figure 2

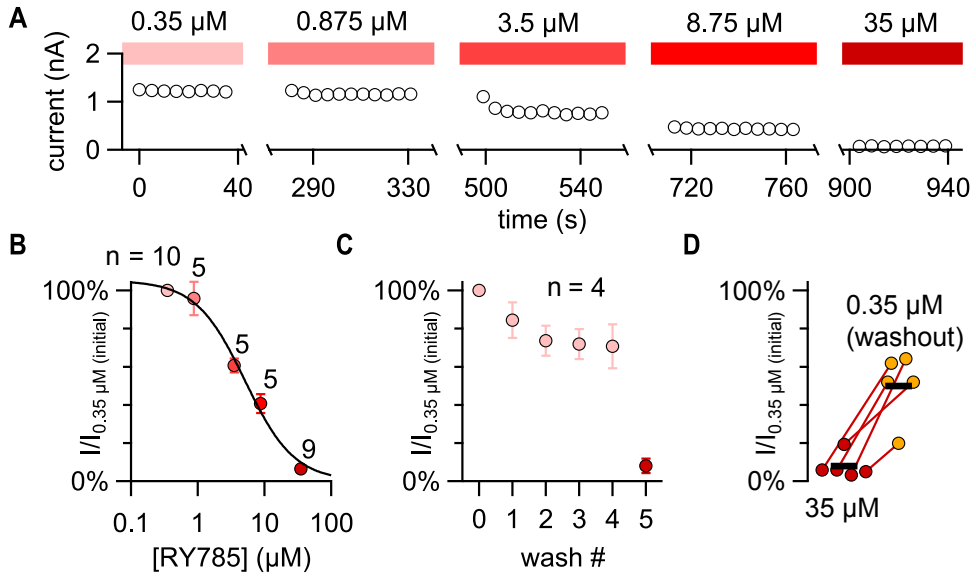

Figure 2. RY785 blocks Kv2.1/Kv8.1 heteromers in a concentration-dependent manner.

A) Current amplitudes during an RY785 concentration-effect experiment on a Kv2.1-CHO cell transfected with Kv8.1. Circles represent tail current amplitudes 2-4 ms into a step to –9 mV following a 200 ms activating step to 71 mV. Voltage protocol was repeated in 5 s intervals. Solution exchanges occurred during the gaps in the time axis. For exemplar current traces, see Figure 2 Supplement and Figure 3.

B) Mean normalized tail current amplitudes with increasing concentrations of RY785. Error bars represent SEMs. Black curve is a fitted Hill function with $n_H = 1$ ($IC_{50} = 5.1 \pm 1.0$ μM, base = 1.0 ± 0.1 %).

C) Vehicle control tail current with repeated solution exchanges (washes) into 0.35 μM RY785, mimicking solution exchanges in panel B. Vehicle control solution exchanges were followed by exchange into 35 μM RY785 (wash #5). Error bars represent SEMs from n = 4 cells.

D) Tail current recovery following solution exchange from 35 μM RY785 into 0.35 μM RY785 (washout). Bars represent mean current amplitudes from n = 5 cells.

Figure 2 Supplement

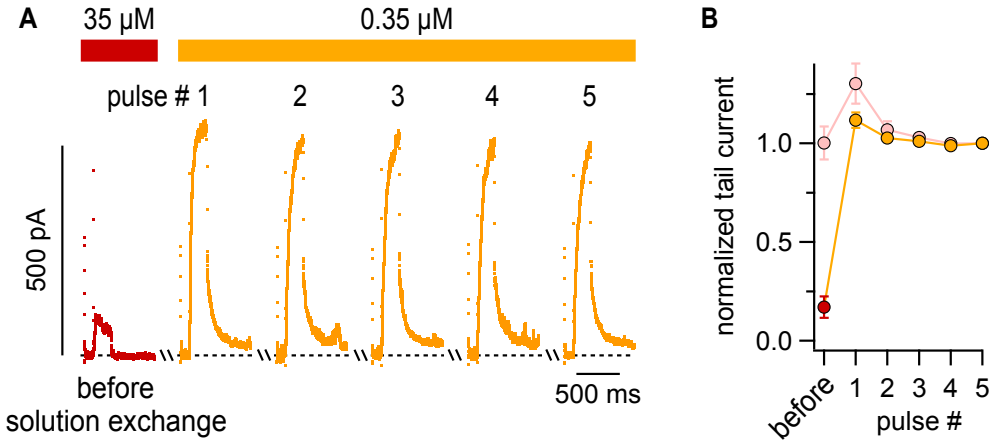

Figure 2 Supplement. Rapid unblock of RY785 from Kv2.1/Kv8.1 heteromers

A) Exemplar traces showing current recovery following solution exchange from 35 µM RY785 into 0.35 µM RY785. Voltage protocol is the same as in Figure 2. Cells were held at -89 mV without pulsing during solution exchange.

B) Tail current amplitudes, as in Figure 2, normalized to pulse #5. n = 5 cells treated first with 35 µM RY785 (dark red) then 0.35 µM RY785 (orange). n = 4 control cells treated first with 0.35 µM RY785 and washed again with 0.35 µM RY785 (pink). The transient increase in current amplitudes upon solution exchange also occurs with Kv2.1 (Marquis and Sack, 2022).

Figure 3

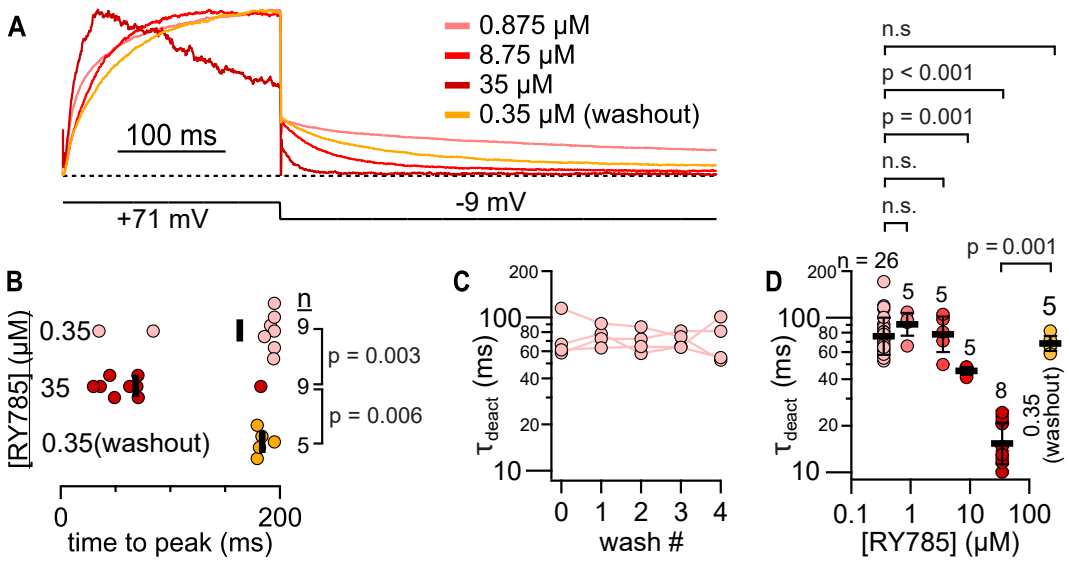

Figure 3. RY785 can affect Kv2.1/Kv8.1 current kinetics.

A) Kinetics of currents from a Kv2.1-CHO cell transfected with Kv8.1 are altered by RY785. Traces normalized to max.
B) Latency to peak current during steps to +71 mV. The time axis of this plot is aligned with that of Panel A. Bars represent means. Unpaired Wilcoxon rank tests.
C) Time constant of deactivation at -9 mV is constant after washes with 0.35 µM RY785. Time constants are derived from fits of a monoexponential function (Equation 3 with A_2 set equal to 0) to tail currents like those shown in Panel A. Fits were from the peak of each tail current to 200 ms after the voltage step. Brown and Forsythe test p = 0.98. ANOVA p = 0.98. Statistics were performed on natural logarithms of time constants. n = 4 cells.
D) RY785 can alter time constant of deactivation. Brown and Forsythe test p = $3x10^{-12}$. Unpaired Welch test p = $1x10^{-7}$. Dunnett tests with 0.35 µM RY785 (initial) as control. Unpaired Wilcoxon rank test comparing 35 µM RY785 to 0.35 µM RY785 (washout) p = 0.001. Statistics were performed on natural logarithms of time constants.

Figure 4

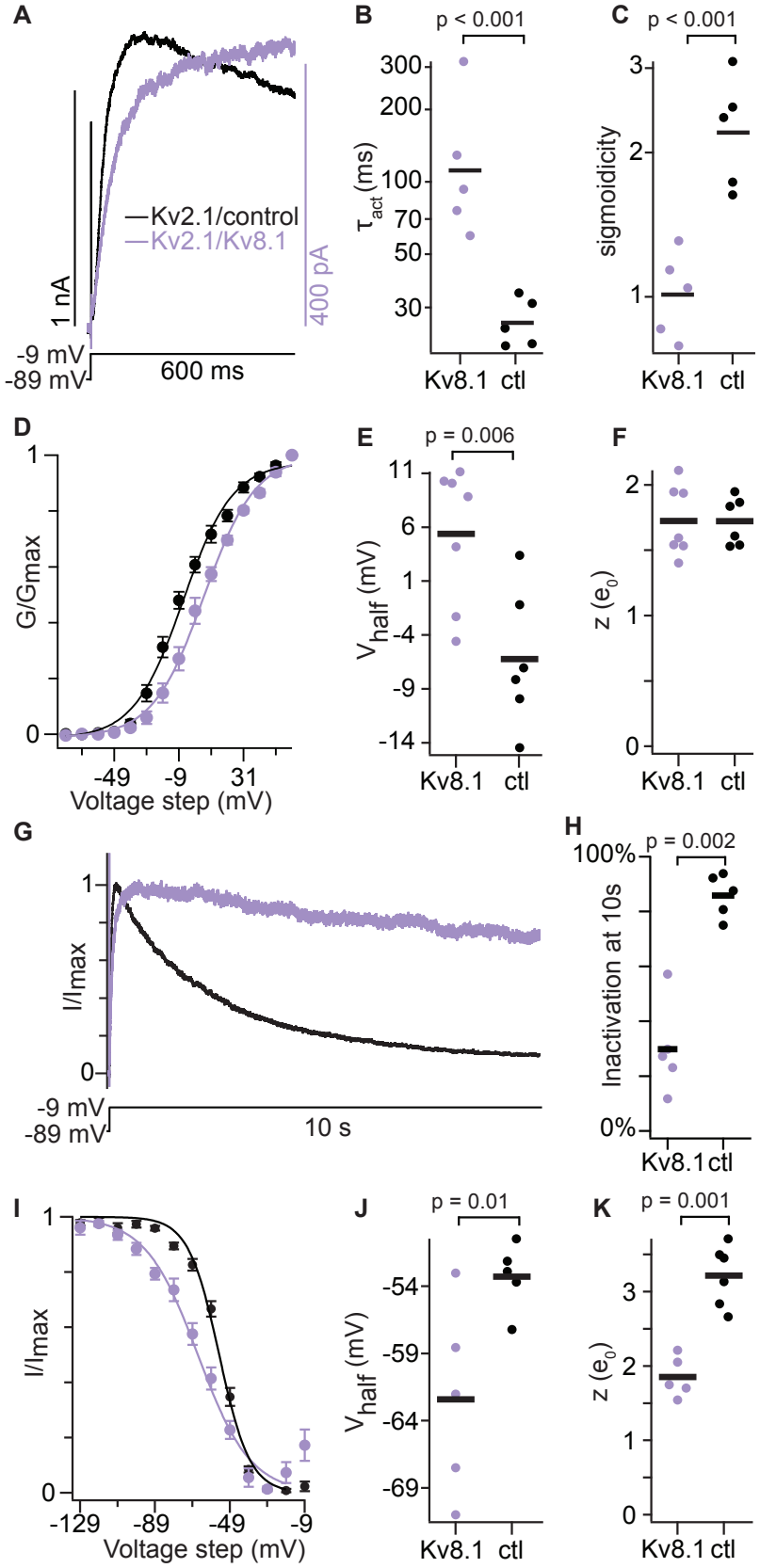
A
1 nA
400 pA
—Kv2.1/control
—Kv2.1/Kv8.1
-9 mV
-89 mV
600 ms
B
p < 0.001
300
200
100
70
50
30
τact (ms)
Kv8.1
ctl
C
p < 0.001
3
2
1
sigmoidicity
Kv8.1
ctl
D
1
0
G/Gmax
-49
-9
31
Voltage step (mV)
E
p = 0.006
11
6
1
-4
-9
-14
Vhalf (mV)
Kv8.1
ctl
F
2
1
0
z (e0)
Kv8.1
ctl
G
1
0
I/Imax
-9 mV
-89 mV
10 s
H
p = 0.002
100%
0%
Inactivation at 10s
Kv8.1
ctl
I
1
0
I/Imax
-129
-89
-49
-9
Voltage step (mV)
J
p = 0.01
-54
-59
-64
-69
Vhalf (mV)
Kv8.1
ctl
K
p = 0.001
3
2
1
0
z (e0)
Kv8.1
ctl

Figure 4. RY785-resistant current is consistent with Kv2.1/Kv8.1 heteromers

Kv2.1/8.1 data (purple) are from Kv2.1-CHO cells transfected with Kv8.1, and are in 1 µM RY785. Kv2.1/control (black) were transfected with Navβ2, and are in vehicle control solution. Before measurements, repeated voltage steps to -9 mV were given until currents stabilized. p values are from two-tailed unpaired Wilcoxon rank test.

A) Exemplar currents during a step to -9 mV.
B) Time constants from exponential fit (Equation 1). Geometric mean.
C) Sigmoidicity from exponential fit (Equation 1). Geometric mean.
D) Conductance-voltage activation relation. Conductance was measured from initial tail currents at -9 mV. Mean ± SEM. Kv2.1/Kv8.1 n = 7 cells Kv2.1 n = 6 cells. Lines are Boltzmann fits (Equation 2) (Kv2.1/Kv8.1: $V_{1/2}$ = 6 ± 1 mV, z = 1.6 ± 0.1 e_0; Kv2.1/control: $V_{1/2}$ = -6.3 ± 1 mV, z = 1.7 ± 0.1 e_0).
E) Activation $V_{1/2}$ values from individual cells.
F) Activation z values.
G) Exemplar currents during a 10 s step to -9 mV.
H) Percent of current inactivated after 10 seconds at -9 mV.
I) Steady state currents at -9 mV after holding at indicated voltages for 10 seconds. Normalized to the max and min. Mean ± SEM. Kv2.1/Kv8.1 n = 5 cells Kv2.1 n = 5 cells. Lines are Boltzmann fits (Equation 2) (Kv2.1/Kv8.1: $V_{1/2}$ = -66 ± 1 mV, z = 1.8 ± 0.1 e_0; Kv2.1/control: $V_{1/2}$ = -54.7 ± 0.8 mV, z = 3.1 ± 0.3 e_0).
J) Inactivation $V_{1/2}$ values from individual cells.
K) Inactivation z values.

Figure 4 Supplement

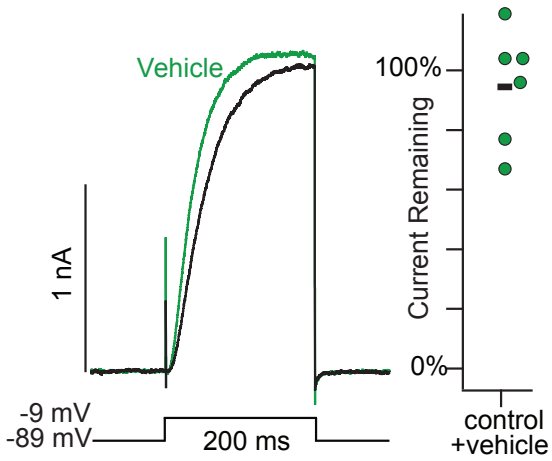

Figure 4 Supplement. Effect of vehicle control on Kv2.1.

Left: Exemplar traces from a Kv2.1-CHO cell transfected with Navβ2. Black and green traces are currents before and after application of vehicle control respectively. Right: Current remaining after application of vehicle control. Black bar represents mean. Each point represents current from one cell at the end of a 200 ms -9 mV voltage step.

Figure 5

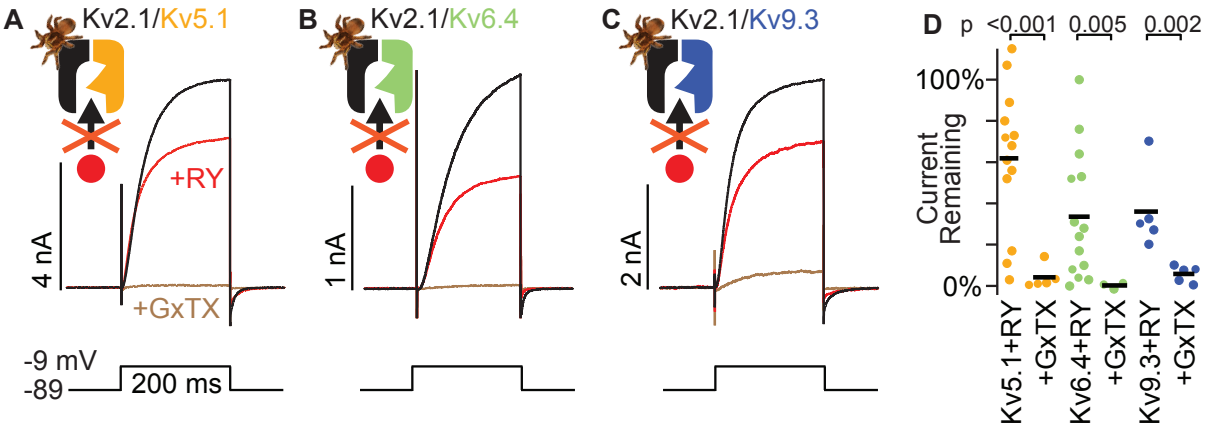

Figure 5. A subunit from each KvS family is resistant to RY785

A) Exemplar traces from a voltage-clamped Kv2.1-CHO cell transfected with Kv5.1. Black and red traces are currents before and after application of 1 µM RY785 respectively. Brown trace is current after subsequent application of 1 µM RY785 + 100 nM GxTX
B) Exemplar traces from a Kv2.1-CHO cell transfected with Kv6.4.
C) Exemplar traces from a Kv2.1-CHO cell transfected with Kv9.3.
D) Current remaining after application of 1 µM RY785 or 1 µM RY785 + 100 nM GxTX. Black bars represent mean. Each point represents current from one cell at the end of a 200 ms voltage step to -9 mV. Unpaired Wilcoxon rank tests.

Figure 6

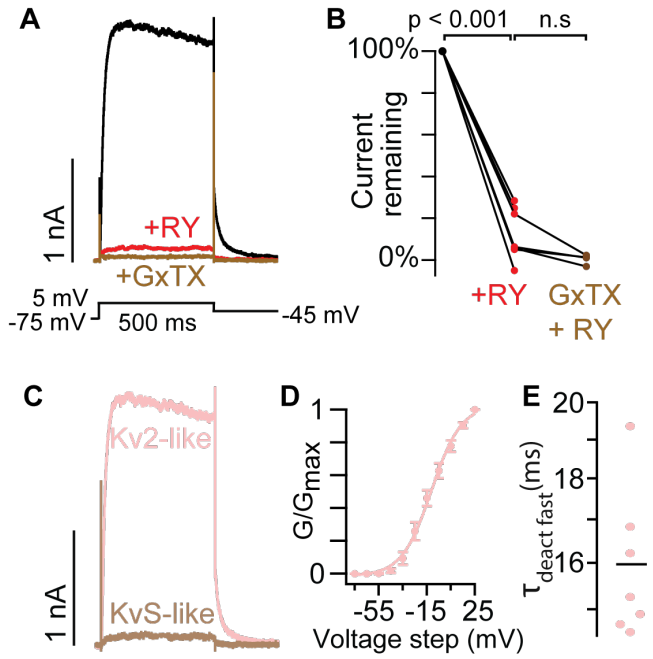

Figure 6. Mouse superior cervical ganglion neurons lack substantial KvS-like currents.

A) Exemplar currents from a voltage-clamped SCG neuron. Black and red traces are currents before and after application of 1 µM RY785 respectively. Brown trace is current after subsequent application of 1 µM RY785 + 100 nM GxTX.
B) Tail current amplitude 10 ms after voltage was stepped from +5 mV to -45 mV normalized to current amplitude before RY785. Paired Wilcoxon rank tests, n = 7 neurons, N = 3 mice.
C) Subtracted currents from A. Kv2-like current is the RY785-sensitive current (black trace minus red in A). KvS-like current is the GxTX-sensitive current remaining in RY785 (red trace minus brown in A).
D) Conductance-voltage activation relation of Kv2-like current in SCG neurons. Conductance was measured from tail currents at -45 mV. $V_{1/2}$ = -11 ± 1 mV, z = 2.1 ± 0.2 e_0 Mean ± SEM. n = 7 neurons, N = 3 mice.
E) The faster time constant of a double exponential (Equation 3) fit to channel deactivation at -45 mV.

Figure 7

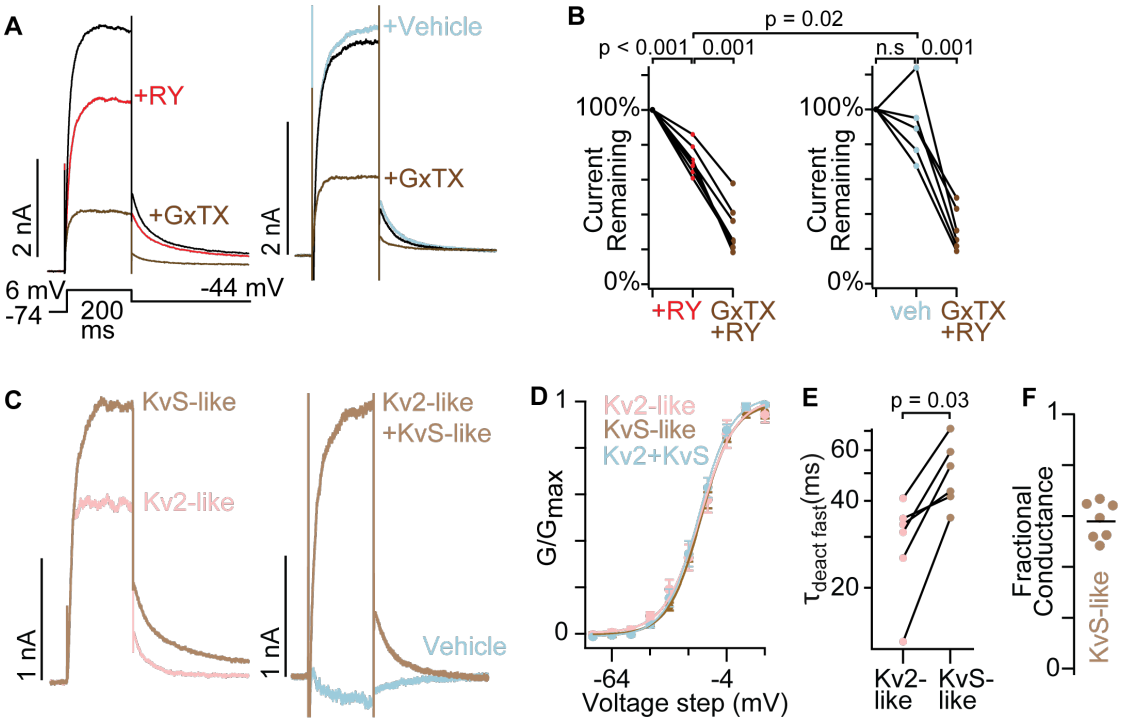

Figure 7. Mouse nociceptors have RY785-resistant KvS-like currents.

A) Exemplar currents from nonpeptidergic nociceptors, GFP^{+} neurons from *Mrgprd*^{GFP} mice.
B) Tail current amplitude 10 ms after voltage was stepped from +6 mV to -44 mV normalized to current amplitude before RY785 or vehicle treatment. Wilcoxon rank tests were paired, except the comparison of RY785 to vehicle which was unpaired. RY785 then GxTX: n = 7 neurons, N = 4 mice. Vehicle then GxTX: n = 6 neurons, N = 4 mice.
C) Exemplar subtracted currents from A. Kv2-like is the initial current minus RY785 (black trace minus red in A left panel). KvS-like is the current in RY785 minus GxTX (red trace minus brown in A left panel). Kv2-like+KvS-like is the current in vehicle minus RY785 + GxTX (blue trace minus brown in A right panel).
D) Voltage dependance of activation of subtraction currents in *Mrgprd*$^{GFP+}$ neurons. Pink points represent Kv2-like currents, brown points represent KvS like currents, and light blue points represent Kv2+KvS-like currents after vehicle treatment. Conductance was measured from initial tail currents at -44 mV. Kv2-like: $V_{1/2}$ = -18 ± 1 mV, z = 2.7 ± 0.3 e_0, KvS-like: $V_{1/2}$ = -18 ± 1 mV, z = 3 ± 0.2 e_0, Kv2 + KvS-like: $V_{1/2}$ = -19 ± 1 mV, z = 2.9 ± 0.1 e_0. Mean ± SEM. KvS-like and Kv2-like n = 7 neurons N = 4 mice, Kv2+KvS-like n = 6 neurons N = 4 mice.
E) The faster time constant of a double exponential fit (Equation 3) to channel deactivation at -44 mV. p value represents paired Wilcoxon rank test.
F) Fractional KvS-like conductance relative to the total RY785 + GxTX-sensitive conductance. KvS-like is only sensitive to GxTX.

Figure 7 Supplement 1

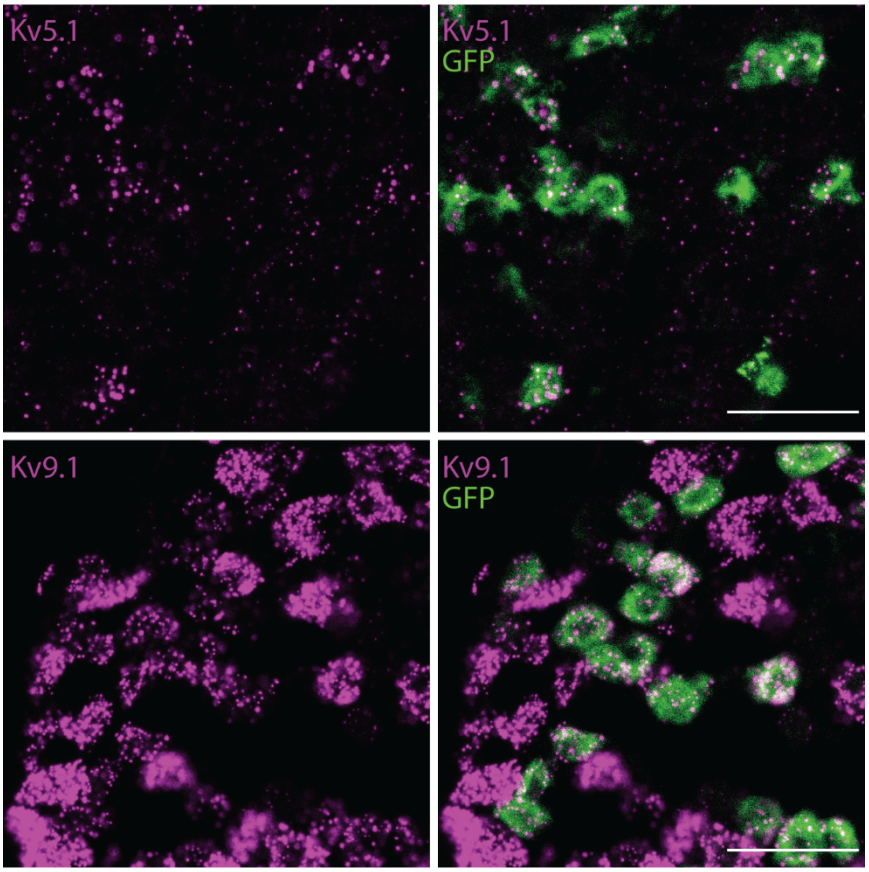

Figure 7 Supplement 1. Nonpeptidergic nociceptors express Kv5.1 and Kv9.1 mRNA transcripts.

Exemplar images of DRG sections from a *Mrgprd*^{GFP} mouse labeled with RNAscope *in situ* hybridization for *KCNF1* (Kv5.1) (top magenta) or *KCNS1* (Kv9.1) (bottom magenta). Scale bars are 50 µm.

Fig 7 Supplement 2

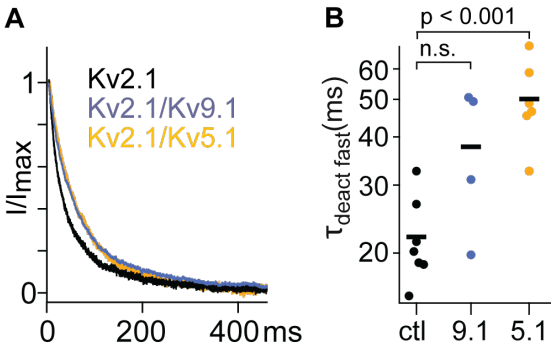

Figure 7 Supplement 2. RY785 resistant currents from Kv2.1-CHO cells transfected with Kv5.1 or Kv9.1 deactivate slower than currents from untransfected Kv2.1-CHO cell.

A) Exemplar traces of channel deactivation at -49 mV after a 50 ms step to +11 mV. Traces are normalized to max current during the -49 mV step.
B) The faster time constant of a double exponential fit (Equation 3) to channel deactivation. Dunnett tests versus control (ctl). Ctl n = 7. Kv9.1 n = 4. Kv5.1 n = 6.

Figure 8

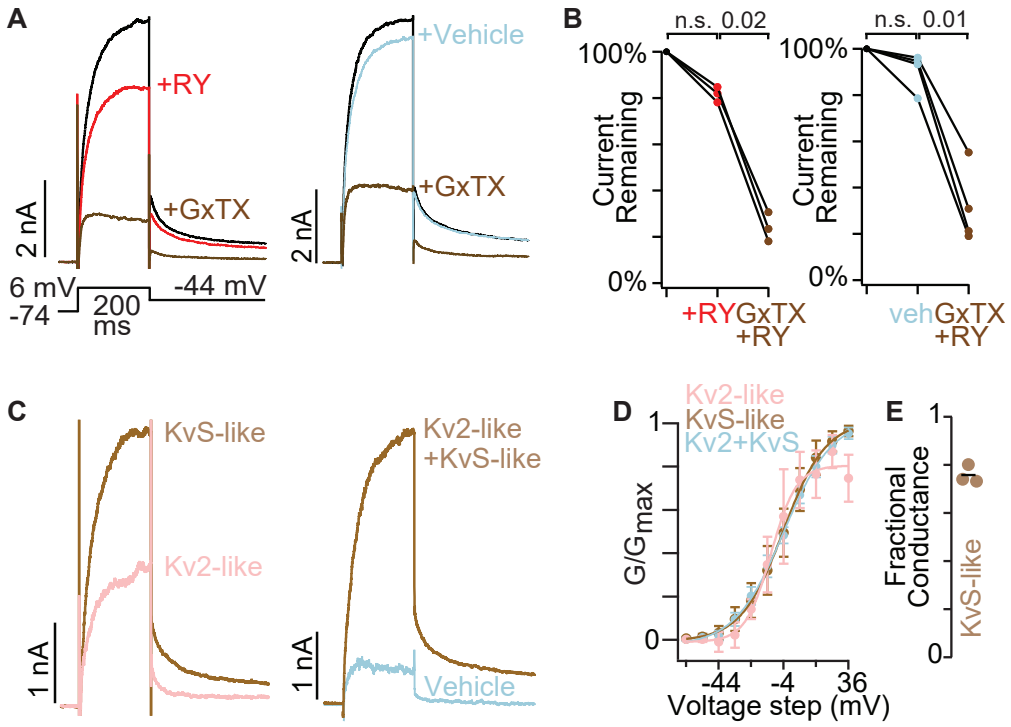

Figure 8. Human somatosensory neurons have RY785-resistant KvS-like currents.

A) Exemplar currents from human dorsal root ganglion neurons.

B) Tail current amplitude 10 ms after voltage was stepped from +6 mV to -44 mV normalized to current amplitude before RY785 or vehicle treatment. Paired Wilcoxon rank tests. RY785 then GxTX: n = 3 neurons. Vehicle then GxTX: n = 4 neurons. All neurons from same human.

C) Exemplar subtracted currents from A. Kv2-like is the initial current minus RY785 (black trace minus red in A left panel). KvS-like is the current in RY785 minus GxTX (red trace minus brown in A left panel). Kv2+KvS-like is the current in vehicle minus RY785 + GxTX (blue trace minus brown in A right panel).

D) Voltage dependence of activation of subtraction currents in human dorsal root ganglion neurons. Pink points represent Kv2-like currents, brown points represent KvS like currents, and blue points represent Kv2 + KvS-like currents after vehicle treatment. Conductance was measured from initial tail currents at -44 mV. Mean ± SEM. Kv2 + KvS-like n = 3 neurons N = 1 human, KvS+Kv2-like n = 4 neurons N = 1 human.

E) Fractional KvS-like conductance relative to the total RY785 + GxTX-sensitive conductance. KvS-like is only sensitive to GxTX.